AD-A189 326 INVESTIGATION OF SURFACE WAVE BLINDNESS IN MICROSTRIP PHASED ARRAY ANTENNAS(U) ROME AIR DEVELOPMENT CENTER GRIFFISS AFB NY D T MCGRATH ET AL. APR 87 1/1

UNCLASSIFIED RADC-TR-87-39 F/G 9/1 NL

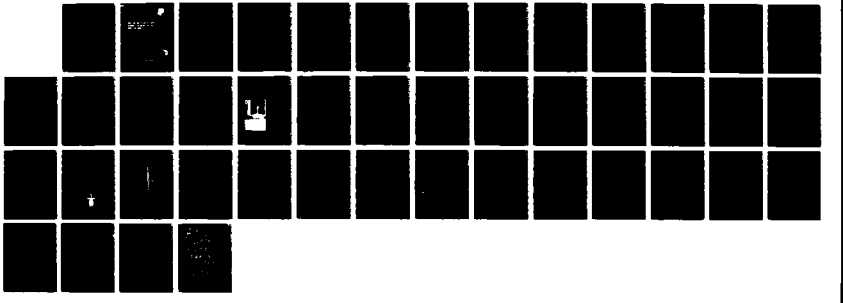

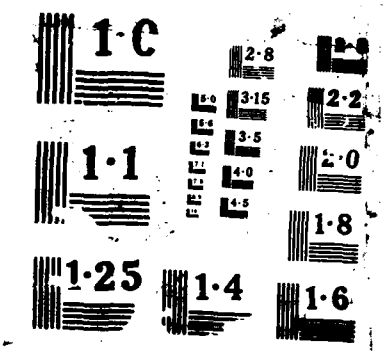
1·C
1·1
1·25
1·4
2·8
3·15
3·5
4·0
4·5
2·2
2·0
1·8
1·6

RADC-TR-87-39
In-House Report
April 1987

INVESTIGATION OF SURFACE WAVE BLINDNESS IN MICROSTRIP PHASED ARRAY ANTENNAS

Daniel T. McGrath, Capt, USAF and Mark R. Fitzgerald, Cadet, USAF

APPROVED FOR PUBLIC RELEASE; DISTRIBUTION UNLIMITED

ROME AIR DEVELOPMENT CENTER
Air Force Systems Command
Griffiss Air Force Base, NY 13441-5700

Unclassified
SECURITY CLASSIFICATION OF THIS PAGE

REPORT DOCUMENTATION PAGE

Form Approved OMB No 0704-0188

1a. REPORT SECURITY CLASSIFICATION: Unclassified	1b. RESTRICTIVE MARKINGS
2a. SECURITY CLASSIFICATION AUTHORITY	3. DISTRIBUTION/AVAILABILITY OF REPORT: Approved for public release; distribution unlimited.
2b. DECLASSIFICATION/DOWNGRADING SCHEDULE	
4. PERFORMING ORGANIZATION REPORT NUMBER(S): RADC-TR-87-39	5. MONITORING ORGANIZATION REPORT NUMBER(S)
6a. NAME OF PERFORMING ORGANIZATION: Rome Air Development Center; 6b. OFFICE SYMBOL (If applicable): RADC/EEAA	7a. NAME OF MONITORING ORGANIZATION
6c. ADDRESS (City, State, and ZIP Code): Hanscom AFB, Massachusetts 01731-5000	7b. ADDRESS (City, State, and ZIP Code)
8a. NAME OF FUNDING/SPONSORING ORGANIZATION; 8b. OFFICE SYMBOL (If applicable)	9. PROCUREMENT INSTRUMENT IDENTIFICATION NUMBER
8c. ADDRESS (City, State, and ZIP Code)	10. SOURCE OF FUNDING NUMBERS

PROGRAM ELEMENT NO.	PROJECT NO.	TASK NO	WORK UNIT ACCESSION NO.
61102F	2305	J3	03

11. TITLE (Include Security Classification): Investigation of Surface Wave Blindness in Microstrip Phased Array Antennas

12. PERSONAL AUTHOR(S): Daniel T. McGrath, Capt, USAF and Mark R. Fitzgerald, Cadet, USAF

13a. TYPE OF REPORT	13b. TIME COVERED	14. DATE OF REPORT (Year, Month, Day)	15. PAGE COUNT
In-House	FROM _____ TO _____	1987 April	46

16. SUPPLEMENTARY NOTATION

17. COSATI CODES			18. SUBJECT TERMS (Continue on reverse if necessary and identify by block number)	
FIELD	GROUP	SUB-GROUP		
09	03		Microstrip antennas	Phased arrays
			Surface waves	Scan blindness
			Leaky waves	Antenna measurements

19. ABSTRACT (Continue on reverse if necessary and identify by block number)

Surface waves and leaky waves are mechanisms through which elements of microstrip phased arrays can couple, potentially causing blind spots in the desired field of view. This report summarizes results of a project whose objective was to verify existing theories predicting blind spot locations. It summarizes the method of solving for blindness angles, the method of measuring scan impedance, and the results of measurements of a microstrip array on a high dielectric constant material.

20 DISTRIBUTION/AVAILABILITY OF ABSTRACT	21 ABSTRACT SECURITY CLASSIFICATION
☐ UNCLASSIFIED/UNLIMITED ☒ SAME AS RPT ☐ DTIC USERS	Unclassified

22a NAME OF RESPONSIBLE INDIVIDUAL	22b TELEPHONE (Include Area Code)	22c OFFICE SYMBOL
Daniel T. McGrath, Capt, USAF	(617) 377-4036	RADC/EEAA

DD Form 1473, JUN 86 — Previous editions are obsolete

SECURITY CLASSIFICATION OF THIS PAGE
Unclassified

Preface

This report summarizes work performed at Rome Air Development Center's Electromagnetics Directorate. Cadet Fitzgerald's participation in these experiments was a result of the United States Air Force Academy's (USAFA) Cadet Summer Research Program. Major Robert Norris was the sponsor for USAFA/DFEE (Dept. of Electrical Engineering). Captain Daniel McGrath was RADC's sponsor and the co-investigator.

The authors thank John McIlvenna and Peter Franchi for their assistance and advice in performing this experiment, James Kenney and Edward Martin for their assistance in making the measurements, and 2 Lt Daniel Mullinix for the experimental data on single microstrip elements.

Contents

Illustrations

Tables

Investigation of Surface Wave Blindness in Microstrip Phased Array Antennas

1. INTRODUCTION

Printed arrays have potential as conformal antennas for airborne communications terminals. The concept of a microstrip array on Gallium Arsenide (GaAs) or Indium Phosphide (InP) is particularly attractive since active devices such as FET (field effect transistor) switches and amplifiers can be constructed monolithically in those materials. Using FET switches for phase shifters and the FET amplifiers for low noise receive amplifiers or high power transmit amplifiers, all the functions of a small phased array can be incorporated on one GaAs or InP layer.[1,2]

A potential difficulty arises when we try to use thick GaAs or InP substrates to obtain wide bandwidth from the microstrip array elements (a microstrip antenna's bandwidth increases along with its thickness).[3] The thick dielectric layer

(Received for publication 14 April 1987)

1. Schindler, J.K. (1985) Performance bounds on monolithic phased array antennas, Phased Arrays 1985 Symposium Proceedings, RADC-TR-85-171, AD A169316, pp. 49-76.

2. Edward, B.J. (1984) Integration of monolithic microwave integrated circuits into phased array antenna systems, Proceedings of the 1983 Antenna Applications Symposium, RADC-TR-84-52, AD A142003, pp. 39-64. Vol. I.

3. Bahl, I.J., and Bhartia, P. (1980) Microstrip Antennas, Artech House.

can support surface waves that provide an added path for mutual coupling between array elements, possibly resulting in scan blindness. The effect is most severe for "electrically thick" (more than $\lambda_o/20$) substrates with high dielectric constants.[4]

To verify theoretical predictions of surface wave blind spots, we built and measured two 16-GHz arrays on 50-mil Epsilam-10®. The arrays did in fact have high reflection coefficients at or near the scan angles predicted by the theory. Yet, there were other deleterious effects in the arrays that caused blind spots in other locations as well. In particular, it appears there was excessive coupling between the microstrip feed lines, suggesting that other parts of monolithic arrays may also interact by way of surface waves.

The original objectives of this project were first, to verify the scan blindness theory experimentally and second, to test possible remedies, such as grooves or other obstructions in the substrate. Although we met the first objective, we postponed the second due to problems encountered with the material properties and microstrip design formulas at the relatively high 16-GHz frequency. This report discusses those difficulties and suggests possible solutions. It reviews the theory of surface wave blindness, and the rationale for our experimental array design. It also describes the experiment procedure, results, and recommendations for further work in this area.

2. SURFACE WAVE BLINDNESS THEORY

2.1 Active Array Reflection

The problem of scan blindness in phased array antennas is well known from many discussions in the literature, for example Lee, Wong and Tang[5] and Oliner.[6] In brief, the interaction between array elements, or mutual coupling, provides a path for transmitted energy to return to the source. As illustrated in Figure 1, the total reflection the source sees is the sum of the direct reflection from the array elements and the coupled energy emitted by the elements, but returning by way of the others instead of radiating out into free space. One consequence of this

4. Pozar, D.M., and Schaubert, D.H. (1984) Scan blindness in infinite arrays of printed dipoles, IEEE Trans. Antennas Propag., AP-32:602-610.

5. Lee, S.W., Wong, N.S., and Tang, R. (1972) Analysis of infinite planar array of rectangular waveguides by generalized scattering matrix approach, Phased Array Antennas, Ed. Oliner and Knittel, Artech House, pp. 91-106.

6. Oliner, A.A. (1972) Surface-wave effects and blindness in phased array antennas, Phased Array Antennas, Artech House, pp. 107-112.

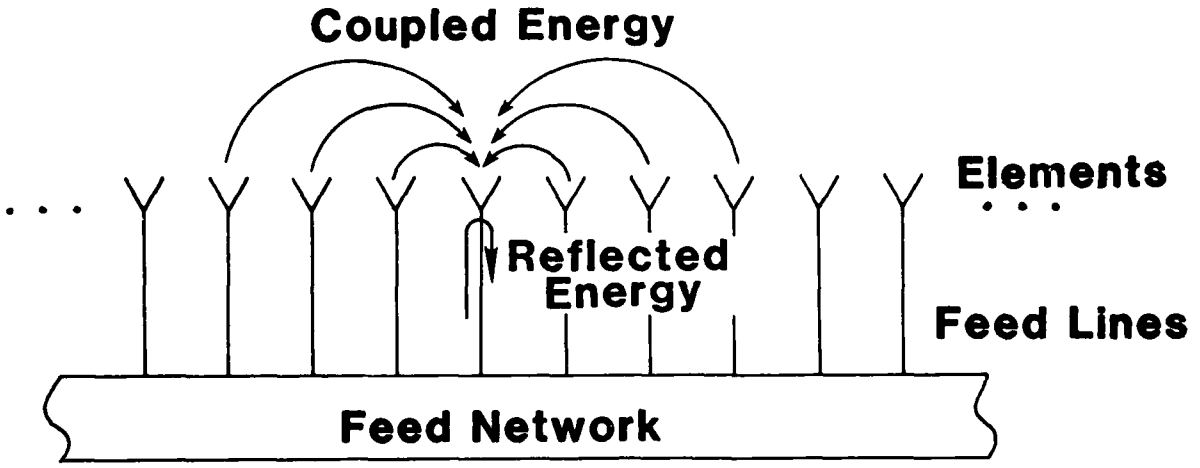

Figure 1. Illustration of Array Reflection (Transmitting Antenna) by Way of Mutual Coupling

phenomenon is that an antenna designed for minimum reflection coefficient as an isolated antenna does not make the best array element. The ideal array element is one that has some reflection equal in magnitude but opposite in phase to the sum of coupled energy. In that situation the array would be perfectly matched even though its elements, if removed from the array, are not.

The active array reflection coefficient, Γ, is defined[7] as:

$$\Gamma_a(\theta,\phi) = \sum_{n=-\infty}^{\infty} S_{on}\, e^{-jk(x_n \sin\theta\cos\phi + y_n \sin\theta\sin\phi)} \qquad (1)$$

where S_{on} is the coupling coefficient between a reference element with coordinates 0,0 and the n'th array element located at x_n, y_n. The wavenumber is k and θ, ϕ are the angles, in spherical coordinates, to which the array is scanned. The array is assumed to be planar, and located in the z = 0 plane. The expression is much simpler for a line-source array with uniform spacing (with elements assumed to be located along the x axis):

$$\Gamma_a(\theta) = \sum_{n} S_{on}\, e^{-jn\,kd\sin\theta} \qquad (2)$$

7. Amitay, N., Galindo, V., and Wu, C. P. (1972) Theory and Analysis of Phased Array Antennas, Wiley.

where d is the interelement spacing. Note that such an array can only scan in the $\phi = 0$ plane. As the array scans, the angles of the coupling coefficient vectors change by kd sin θ, and although the array may be perfectly matched at broadside, there may be angles at which Γ is very close or equal to one. In those cases, the array is said to be blind and it will neither transmit to, nor receive from that blindness angle. Blind spots occur most commonly in arrays with interelement spacings greater than $\lambda/2$, usually just inside the endfire grating lobe angle (exceptions have been noted for some waveguide and dipole arrays[8]:

$$\theta_{EGL} = \sin^{-1}(\lambda/d - 1) . \tag{3}$$

When the array is scanned to that angle, the grating lobe would just begin to appear at endfire. Unless the array structure is loaded with some kind of obstacles or with dielectric, the phases of the coupling coefficient S_{on} depend primarily on the free space distance between elements. But when a dielectric layer is present over the array surface, the elements can also couple through the dielectric with a different propagation phase (a "slow" wave). Consequently, an array blindness due to the surface wave could appear inside the scan region even with array spacings less than 0.5λ.

2.2 Surface Wave Blindness

According to Pozar and Schaubert[4,9] a surface wave blind spot will appear when the surface wave propagation constant equals that of a "Floquet mode:"

$$\beta_{SW} = \beta_{FM} . \tag{4}$$

(Floquet modes are a generalized tool for infinite array analysis, in which we divide the region in front of the array into waveguides with phase shift walls. Floquet modes are like transverse waveguide modes that describe propagation across the array surface.) The Floquet mode propagation constant, normalized to the free space wavenumber, is:

---

8. Mailloux, R.J. (1982) Phased array theory and technology, Proc. IEEE, 70:246-292.

9. Pozar, D.M., and Schaubert, D.H. (1984) Analysis of an infinite array of rectangular microstrip patches with idealized probe feeds, IEEE Trans. Antennas Propag., AP-32:1101.

$$\left[\frac{\beta_{FM}}{k_o}\right]^2 = \left[\frac{m\lambda}{d_x} + u\right]^2 + \left[\frac{n\lambda}{d_y} + v\right]^2 \qquad (5)$$

$$u = \sin\theta\cos\phi \quad ; \quad v = \sin\theta\sin\phi$$

where m and n are arbitrary positive integers and d_x and d_y are the spacings between elements in the x and y directions, respectively, in a planar array located in the z = 0 plane. The surface wave propagation constants, β_{SW}, can be determined approximately from the TE and TM "surface wave functions":[4]

$$T_e = k_1 \cos(k_1 d) + j k_2 \sin(k_1 d) \qquad (6a)$$

$$T_m = \epsilon_r k_2 \cos(k_1 d) + j k_1 \sin(k_1 d) \qquad (6b)$$

where d is the substrate thickness, ϵ_r is its dielectric constant and:

$$k_1^2 = \epsilon_r k_o^2 - \beta^2 \quad ; \quad k_2^2 = k_o^2 - \beta^2 \ .$$

Solving for $T_e = 0$:

$$k_1 \cos(k_1 d) = -j k_2 \sin(k_1 d) \qquad (7a)$$

$$\tan(k_1 d) = -j\sqrt{[\epsilon_r - (\beta/k_o)^2]/[1 - (\beta/k_o)^2]} \qquad (7b)$$

yields the transcendental equation:

$$\tan(2\pi d/\lambda)\sqrt{\epsilon_r - (\beta/k_o)^2} = -\sqrt{[\epsilon_r - (\beta/k_o)^2]/[(\beta/k_o)^2 - 1]} \ . \qquad (8)$$

A similar solution for $T_m = 0$ yields a second transcendental equation for the TM modes:

$$\tan(2\pi d/\lambda)\sqrt{\epsilon_r - (\beta/k_o)^2} = \epsilon_r \sqrt{[(\beta/k_o)^2 - 1]/[\epsilon_r - (\beta/k_o)^2]} \ . \qquad (9)$$

Appendix A discusses the origin of the TE and TM wave functions given above, and shows that they are strictly valid only for an unloaded grounded dielectric. When we load the surface with patch elements and transmission lines, the surface impedance changes. However, when we have a high dielectric constant, the

patches and feed lines take up very little of the surface area and these wave functions should be able to predict approximately the surface wave propagation constant.

The roots of the above two equations give the propagation constants of the TE and TM surface wave modes for any dielectric with thickness d and relative permittivity ϵ_r. For example, with $\epsilon_r = 2.55$ and $d = 0.19\lambda$, there is a TM solution for $\beta/k_o = 1.283$, but no TE solution. It is, in fact, most difficult to excite a TE surface wave mode: for instance, with $\epsilon_r = 10$ the lowest order TE mode does not propagate unless the substrate is more than 0.083λ thick. This is consistent with Harrington's analysis of a dielectric-coated conductor.[10] He gives the cutoff frequencies of the surface wave modes as

$$f_c = \frac{nc}{4d\sqrt{\epsilon_r - 1}} \tag{10}$$

where c is the speed of light in free space and n = 0, 2, 4,... for TM modes and n = 1, 3, 5,... for TE modes. There is no cutoff for the TM_o mode. For higher order modes and certain interesting substrates the cutoff frequencies are listed in Table 1.

Table 1. Surface Wave Mode Cutoff Frequencies

Material, ϵ_r	d (in.)	f_c (GHz)		
		TE_1	TM_2	TE_3
PTFE, 2.54	0.0625	38.04	76.09	114.13
PTFE, 2.54	0.125	19.02	38.04	57.06
Epsilam 10, 10.0	0.025	39.34	78.69	118.03
Epsilam 10, 10.0	0.050	19.67	39.34	59.01
GaAs, 12.8	0.004	214.75	429.49	644.24
GaAs, 12.8	0.010	85.90	171.80	257.70

10. Harrington, R. F. (1961) Time-Harmonic Electromagnetic Fields, McGraw-Hill, pp. 169-170.

The blind spot caused by the TM_o surface wave appears in the E plane.[4] With m = -1 and n = 0. Eq. (4) reduces to

$$(\beta_{SW}/k_o)^2 = (\sin\theta - \lambda/d_x)^2 \ . \tag{11}$$

The surface wave blindness angle is then given by

$$\theta_{SWB} = \sin^{-1}(\lambda/d_x - \beta_{SW}/k_o) \ . \tag{12}$$

Table 2 gives β_{SW}/k_o and the blindness angle for several different dielectrics and frequencies. Figure 2 is a graph of β_{SW}/k_o vs frequency for those materials. Figure 3 shows the blindness angle vs frequency in the E plane due to the TM_o surface wave mode. Curves for Gallium Arsenide are included because 4 mil and 10 mil GaAs are substrates we consider the best choices for monolithic arrays at 20, 44 and 60 GHz. The other materials are those we have available for experimentation. Based on these curves, we selected 0.050 in. thick Epsilam-10 and 16 GHz for our experimental array, to allow us to observe the surface wave blindness at a 45° scan angle, while staying well within the limits (20 GHz) of our measurement equipment.

Table 2. Surface Wave Propagation Constant and Blindness Angle Values Assume Element Spacing of 0.5 λ

	$\epsilon_r = 10.0$				$\epsilon_r = 2.54$			
	d = 0.025 in.		d = 0.050 in.		d = 0.0625 in.		d = 0.125 in.	
f_{GHz}	β_{SW}/k_o	θ	β_{SW}/k_o	θ	β_{SW}/k_o	θ	β_{SW}/k_o	θ
8.0	1.0049	84.3	1.0242	77.4	1.0134	80.6	1.0580	70.4
10.0	1.0080	82.8	1.0452	72.7	1.0213	78.1	1.0940	65.0
12.0	1.0120	81.1	1.0826	66.6	1.0313	75.6	1.1381	59.5
14.0	1.0173	79.4	1.1533	57.9	1.0435	73.0	1.1869	54.4
16.0	1.0242	77.4	1.2892	45.3	1.0580	70.4	1.2359	49.8
18.0	1.0333	75.2	1.5121	29.2	1.0748	67.7	1.2814	45.9

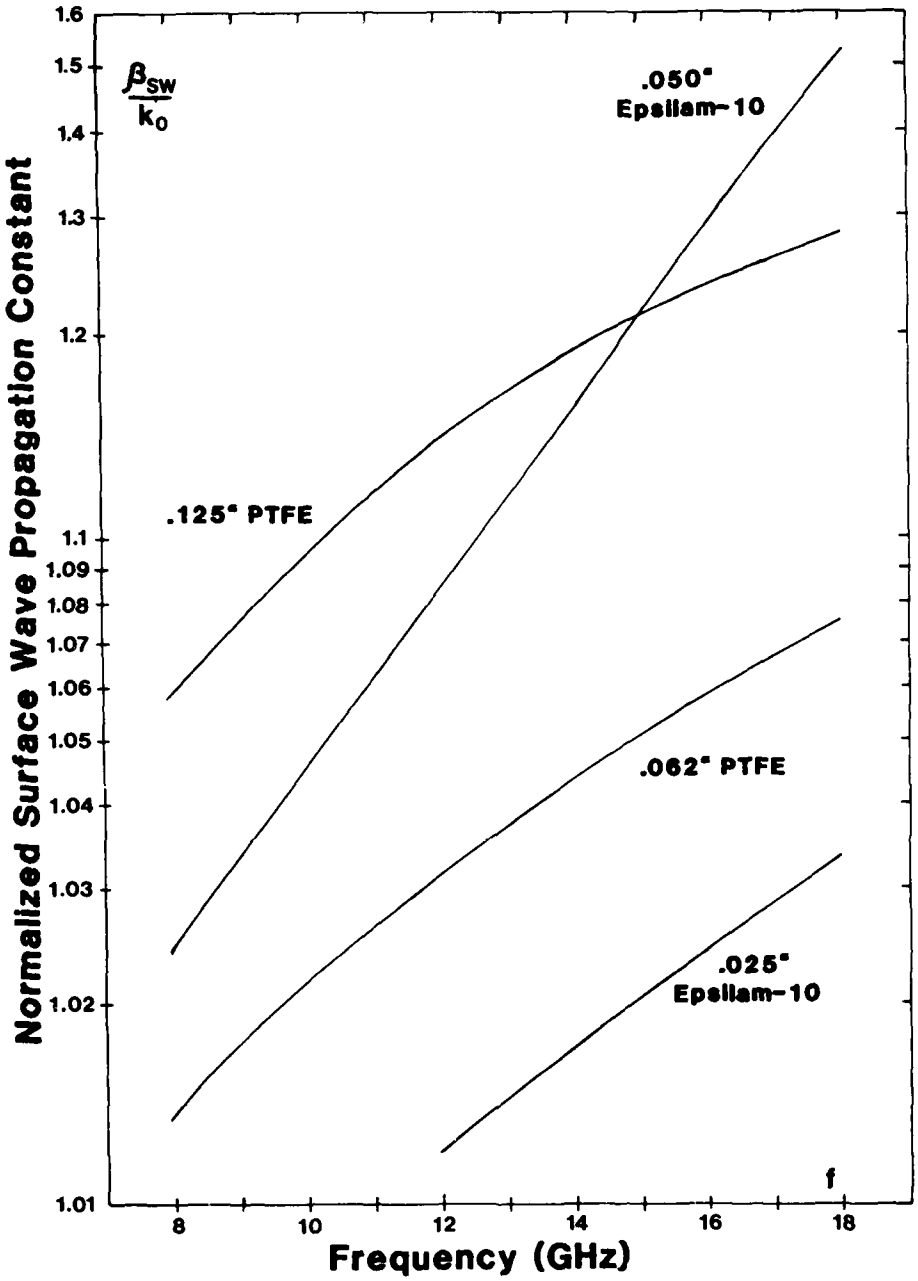

Figure 2. Normalized Surface Wave Propagation Constant vs Frequency for ϵ_r = 2.54, 10.0 and 12.9

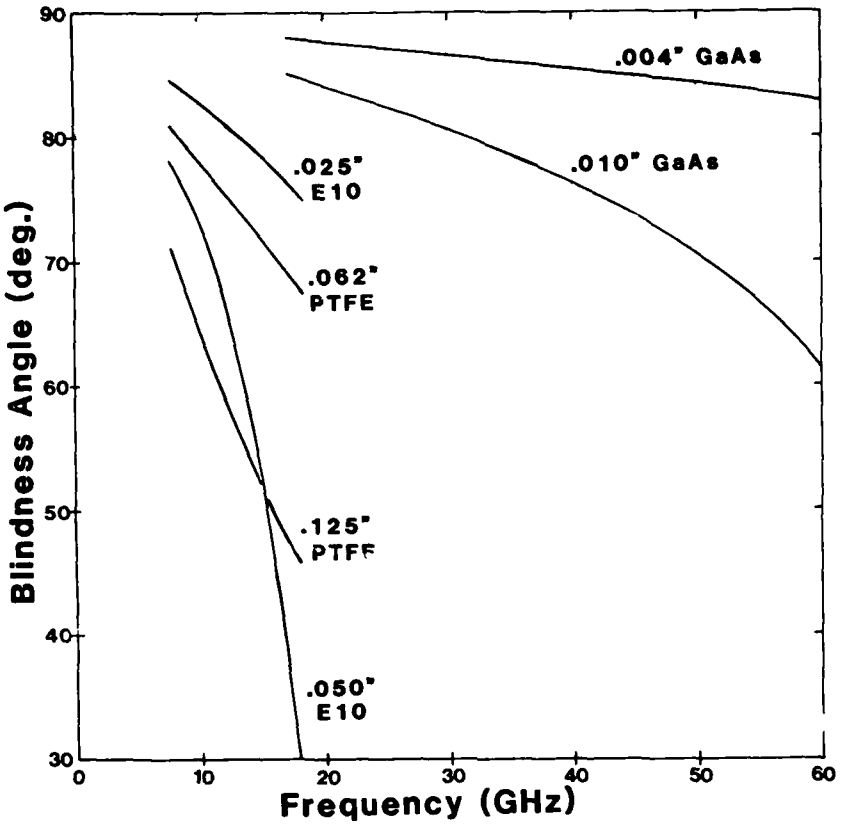

Figure 3. Angle of Surface Wave Blind Spot vs Frequency for ϵ_r = 2.54, 10.0 and 12.9; 0.5 λ Element Spacing

It is encouraging to note that there is no surface wave blindness inside ± 60° for either 4 mil or 10 mil Gallium Arsenide even at frequencies as high as 60 GHz. Since Indium Phosphide's dielectric constant (12.4) is even lower than Gallium Arsenide's (12.9) we need not worry about surface wave blindness for that material either.

3. EXPERIMENT

3.1 Initial Array Design

The initial array design is shown in Figure 4. It is a 22-element E plane array of inset-fed microstrip patch radiators. The patches are fed by microstrip transmission lines whose characteristic impedance is 50 Ω. On this high dielectric constant material the microstrip line is nearly the same width as the center conductor of an SMA coaxial connector. This allowed us to simply solder SMA jack/tab

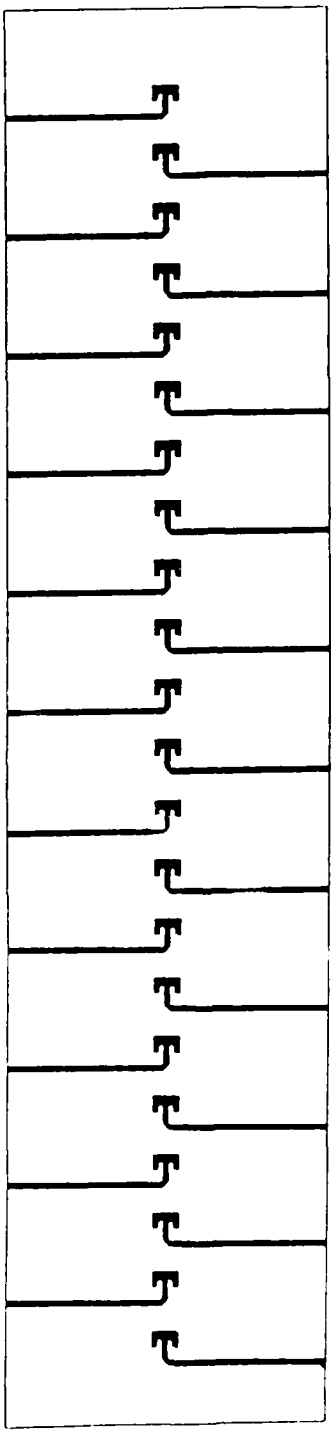

Figure 4. Array Mask Artwork

connectors to the substrate edge without the need for any matching transformer or other transition. On the other hand, the SMA connector flange is wider than the interelement spacing, so we had to feed the elements from alternating edges of the board.

The purpose of the inset region is to impedance match the 50 Ω line to the patch. Ordinarily, the patch's input impedance is near 250 Ω at the edge, but we can inset the feed line to get to the 50-Ω input point.[11, 12] However, it appears the technique did not work with this array, possibly because the inset region is too wide. We found that the only apparent resonant frequency the elements had was near 18 GHz. However, by closing off the inset region with copper tape as shown in Figure 5, we achieved a fairly consistent resonance around 16.2 to 16.3 GHz.

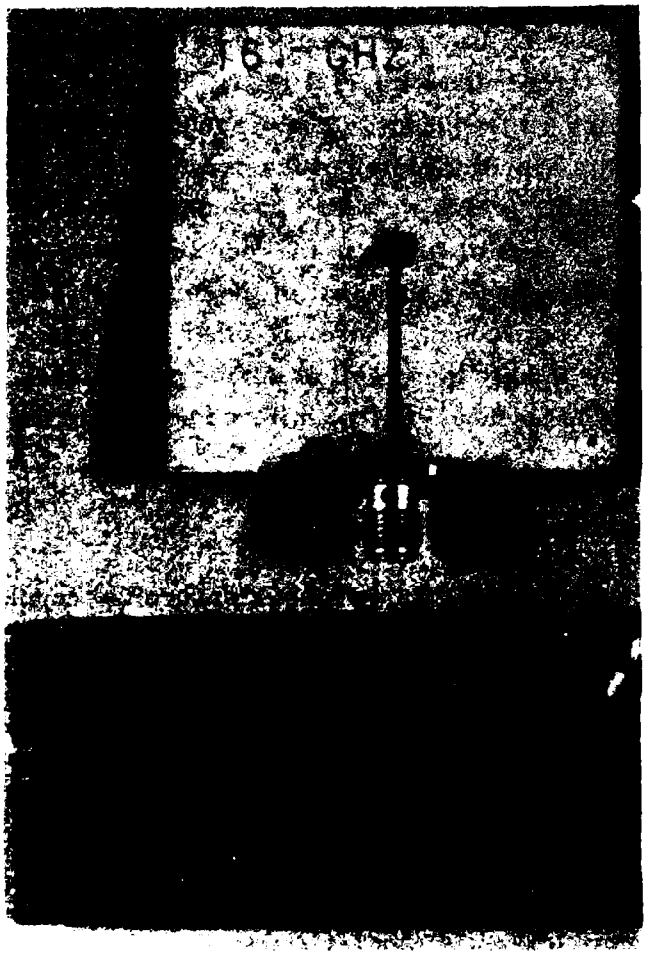

Figure 5. Element With Filled Inset Region

11. Carver, K.R., and Mink, J.W. (1981) Microstrip antenna technology, IEEE Trans. Antennas Propag., AP-29:2-24.

12. Mullinix, D.A., and McGrath, D.T., Capt., (1986) Rectangular Microstrip Patch Antenna Arrays, RADC-TR-86-151.

Figure 6 shows the convention we use to identify elements of the array. Since two identical arrays were constructed, they are labeled "A" and "B" and the inputs are labeled by which side of the array they enter from, "L" or "R" for left or right, respectively. Both arrays were etched side by side on the same piece of material at the same time to minimize variation between them. Also etched on the same piece of Epsilam 10 were several single microstrip patch elements and a straight length of transmission line. Measurements on those components will also be discussed in this report. After photoetching, the two arrays were trimmed to size and SMA connectors were soldered to the feed lines.

3.2 Resonant Frequency

Reflection was measured for each element using the HP8408A R Automatic Network Analyzer. During this test, as in all others discussed in this report, the elements not being measured were terminated with 50 Ω loads. Figure 7 shows a few examples of measured return loss vs frequency. The resonance was much deeper (higher return loss) for elements near the center of the arrays. The return loss at resonance was typically 10 to 20 dB, which we would ordinarily consider quite poor. However, this is the consequence of filling in the feed line inset—the input impedance at the patch edge is much greater than that of the feed line, and the resulting mismatch causes the low return loss. There are other apparent resonances below 16 GHz, but those are mostly the result of series mismatches (destructive interference) between the SMA connector, the mitered bend, and the patch input.

3.3 Active Array Reflection Measurements

To calculate the active reflection coefficient, Γ, we must measure the coupling coefficients, which is straightforward when using a network analyzer. Figure 8 shows the setup for measuring S_{00}, the reflection from the reference element. Figure 9 shows the setup for measuring $S_{0,2}$, that is the transmission from the reference element to the second element away on the right. It is extremely important to note the position of the "reference plane" in these measurements.

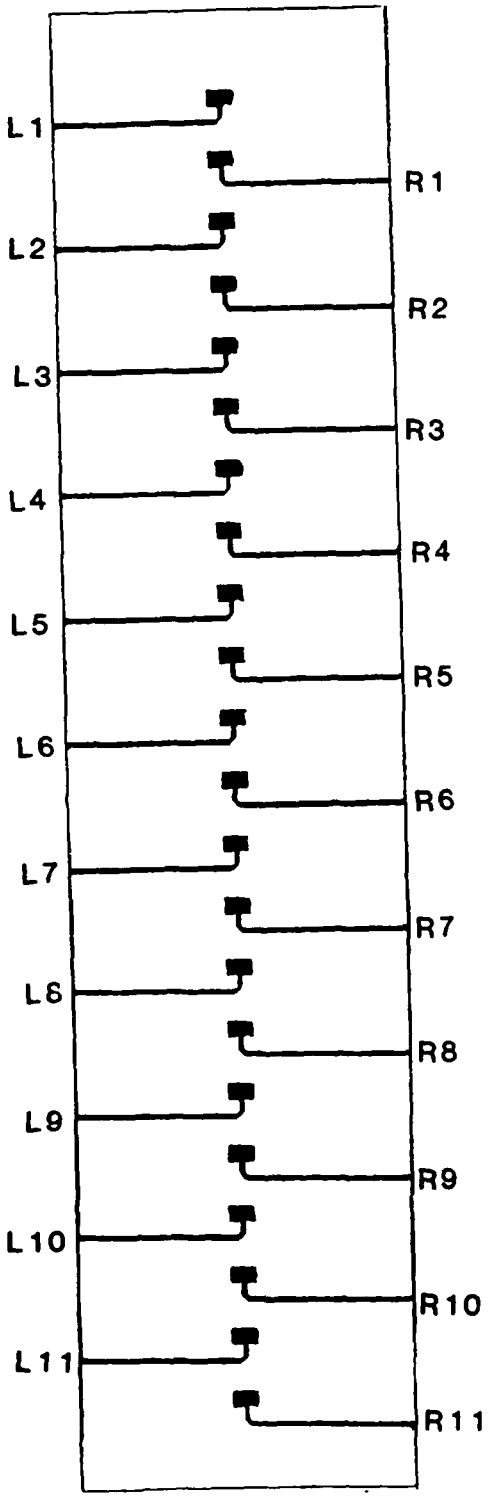

Figure 6. Array Labeling Convention

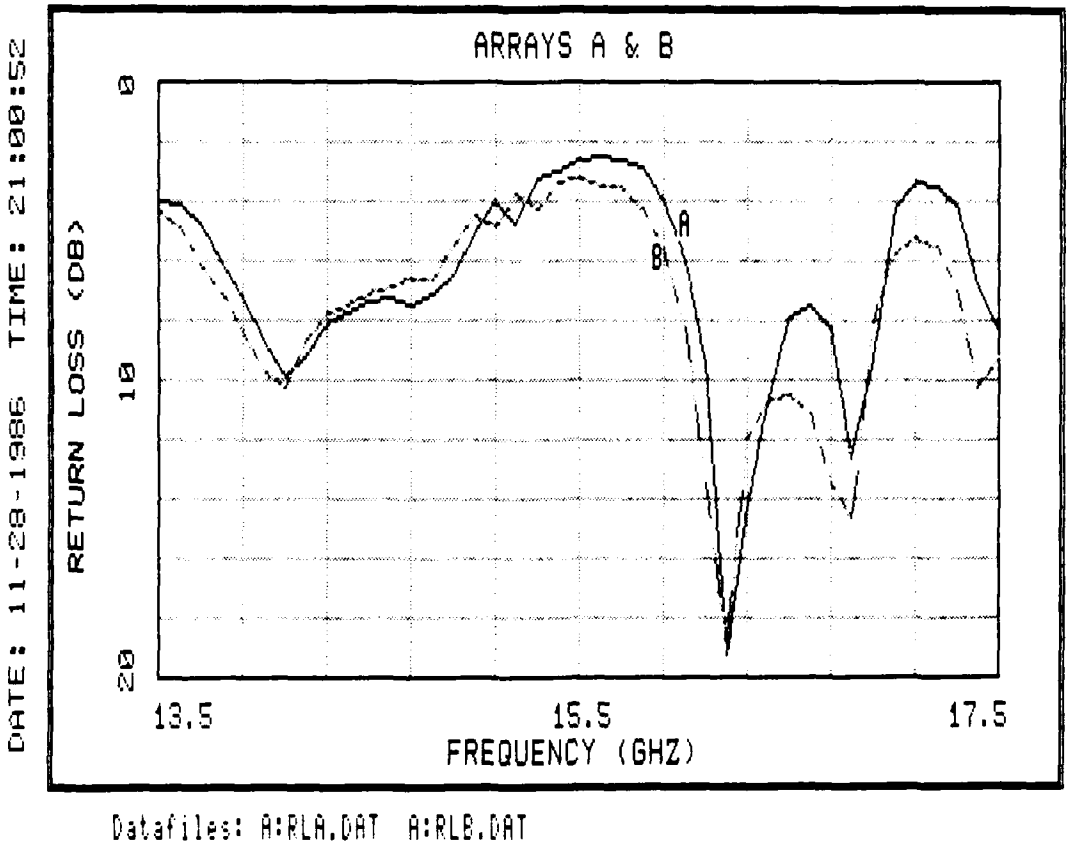

Figure 7. Typical Return Loss vs Frequency for Arrays A & B (Measured S_{00} from AL7 and BL7)

When calibrating for a reflection measurement, we attach a short, a shielded open, and a sliding load directly to the end of the measurement cable that will be connected to the array. Consequently, the reference plane will be at the top surface of the connector jack. On the other hand, when calibrating for a transmission measurement, we insert an adapter (a "bullet" or "thru") between the two measurement cables. Thus the reference plane will be one-half the adapter's length into the probes' input jacks. Since we need to add reflection and coupling terms vectorially, that discrepancy is unacceptable. However, we can correct the measured data by substracting the phase length of the bullet from the coupling terms, or adding it to the reflection term. The bullet used in the thru calibration (OSM217®) has an electrical length of 0.495 inches. The proper phase correction is a function of frequency:

$$\phi = 360^\circ \ell_e/\lambda \quad 360^\circ \ell_e f/c \ . \tag{13}$$

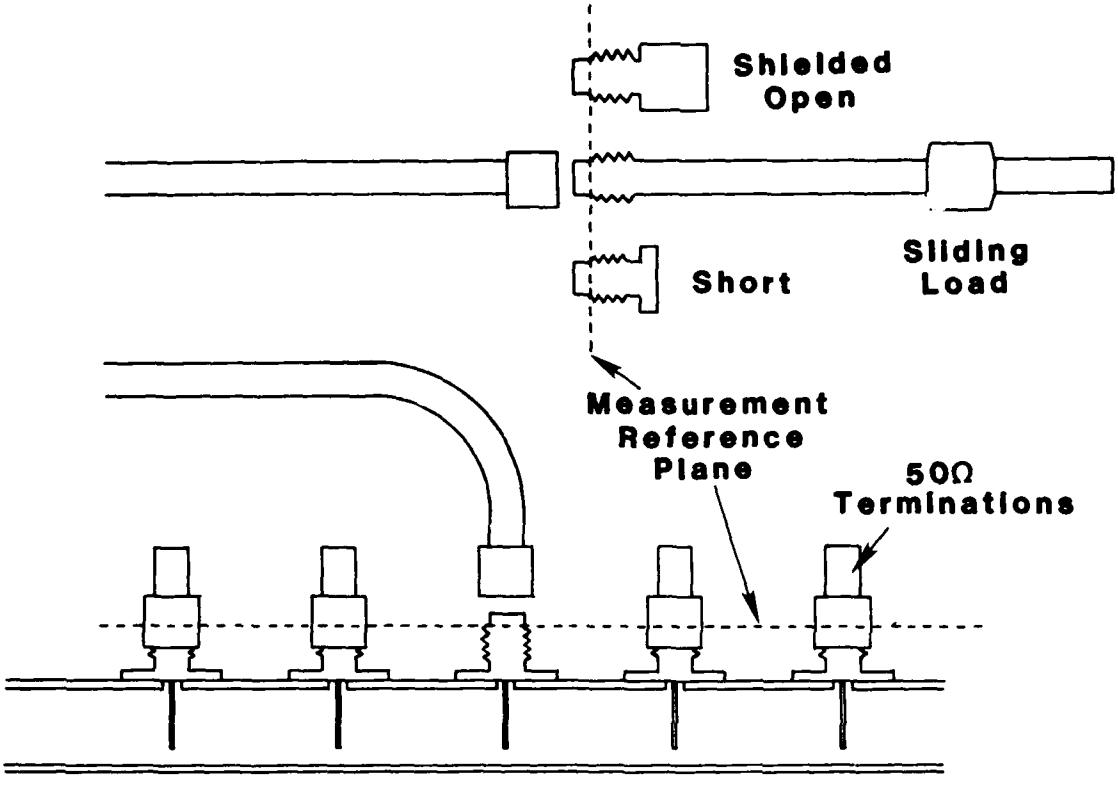

Figure 8. Setup for Measurement of Reflection ($S_{0,0}$) With Automatic Network Analyzer

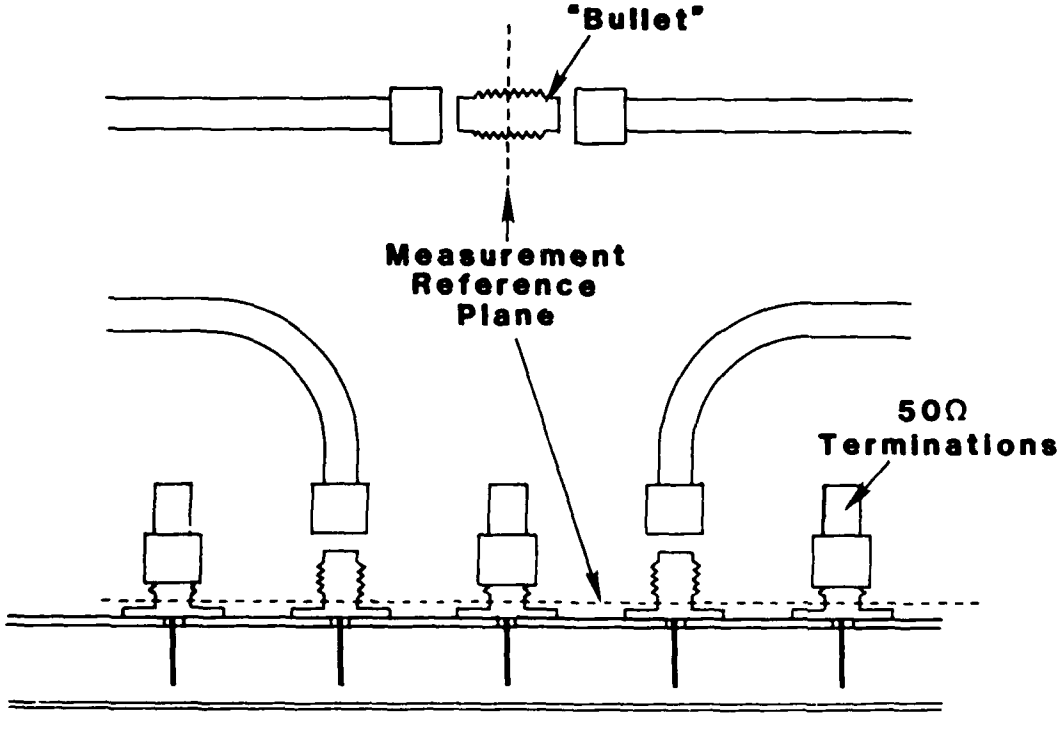

Figure 9. Setup for Measurement of Transmission ($S_{0,2}$) With Automatic Network Analyzer

Table 3 shows examples of the measured coupling data for Array A at 16.2 and 16.3 GHz. Note the corrected reflection phase in parentheses. Figure 10 shows the calculated broadside active reflection coefficient $\Gamma(0)$ vs frequency for the two arrays. Although array A is clearly actively matched at 16.2 GHz, array B does not appear to be matched at any frequency. We are not certain what causes this discrepancy, but offer the following as the most probable reason: Figures 11a and 11b show the calculated reflection coefficient vs scan angle for the two arrays at 16.3 GHz. The difference is most drastic at broadside scan, and may be due to the fact that the feed lines for adjacent pairs of elements enter from opposite sides of the substrate. The parallel microstriplines may couple through a surface wave on their way from the coaxial connectors to the radiators. There would then be some excess coupling between elements fed from the same side of the board (refer to Figures 4 or 6). Figures 12a and 12b show the magnitude of the coupling coefficients, which we normally expect to decrease smoothly going away from the reference element. However, we note that there is stronger coupling between elements fed from the same side of the substrate, and weaker coupling between elements fed from opposing sides. This effect is much more pronounced in Array B for reasons we do not know. Since that excess coupling is between elements located over 1λ apart, we would expect it to produce a blindness near broadside [see Eq. (3)].

Table 3. Measured Coupling Data From Array A

	16.25 GHz		16.30 GHz		16.35 GHz	
S(0, -5)	40.9	154	37.6	- 23	31.2	- 97
S(0, -4)	23.5	-118	22.9	-166	22.5	145
S(0, -3)	33.3	85	23.1	34	22.2	- 15
S(0, -2)	22.1	113	25.4	124	24.4	130
S(0, -1)	16.4	141	16.0	100	16.4	65
S(0, 0)	14.6	-157(88)	17.5	-155(91)	17.0	-177(70)
S(0, 1)	14.4	-143	14.7	169	15.3	122
S(0, 2)	20.3	107	25.9	105	23.8	146
S(0, 3)	22.7	- 22	33.2	6	24.1	16
S(0, 4)	26.0	-155	27.0	-174	25.1	153
S(0, 5)	28.4	-112	31.0	-155	37.8	153

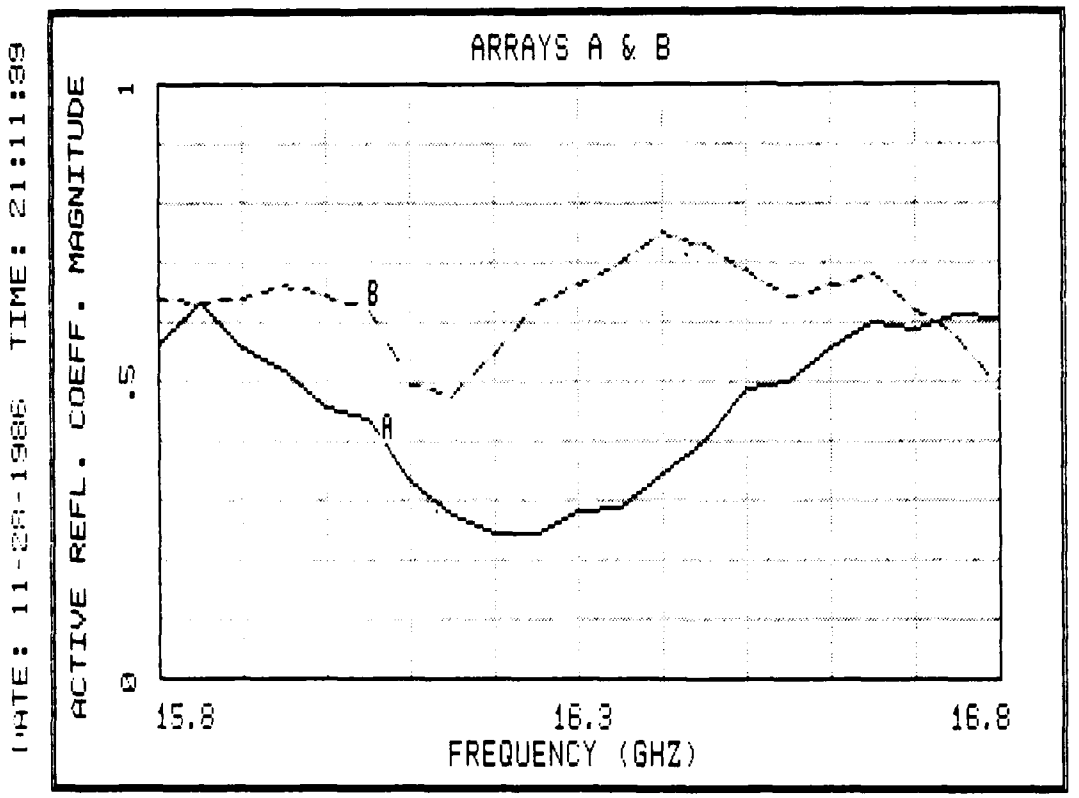

Figure 10. Broadside Scan Active Reflection Coefficient Magnitude $|\Gamma(0)|$ vs Frequency for Arrays A and B

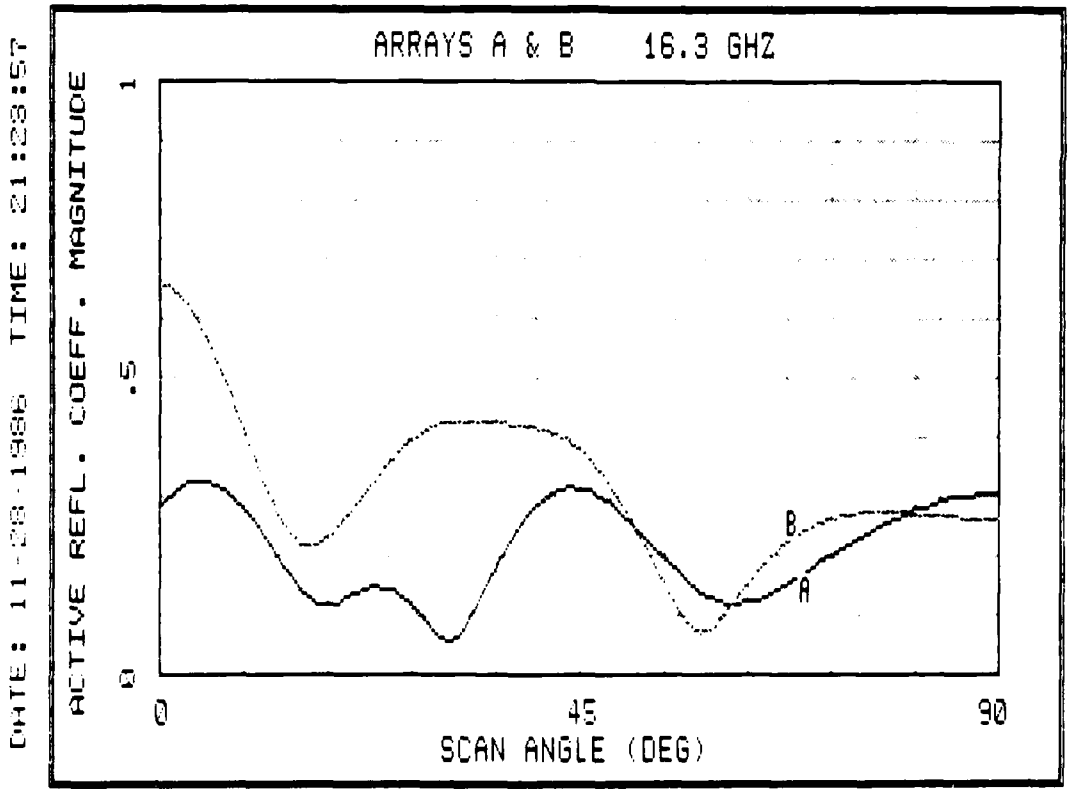

Figure 11. Reflection Coefficient Magnitude vs Scan Angle at 16.3 GHz for Arrays A and B

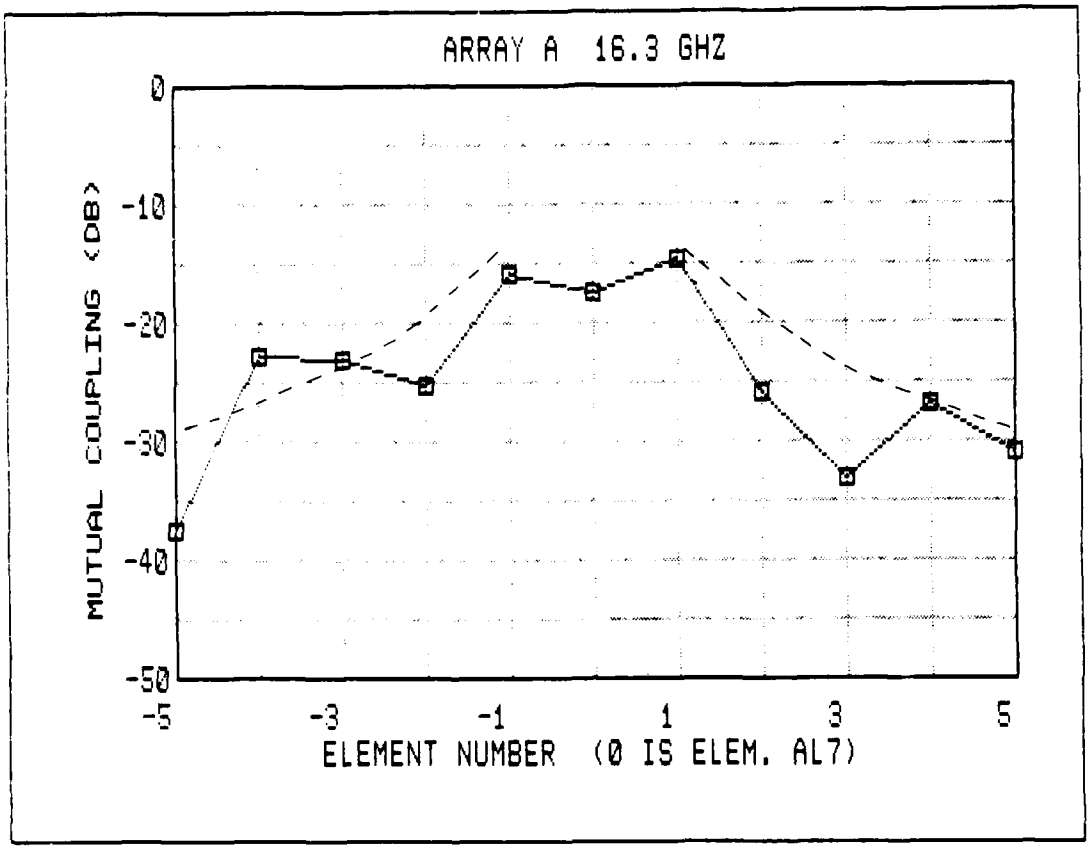

Figure 12a. Coupling Coefficient Magnitudes, $|S_{o,n}|$ From Array A (dashed line is typical microstrip array)

Figure 13a and 13b show Γ vs scan angle for 16.2, 16.25 and 16.3 GHz for Arrays A and B, respectively. In all cases there is a significant increase in Γ near the predicted scan blindness angle of 45°. It is, however, far from convincing since it is not a complete blindness, that is $\Gamma = 1$. However, since there is some attenuation in the microstrip transmission lines leading from the coaxial connectors to the patch elements that we have not subtracted from the measurements, we cannot expect more than $\Gamma = 0.8$ since the two-way line loss is about 2 dB. Although this experiment did appear to show the scan blindness effect we were looking for, the results were far from conclusive.

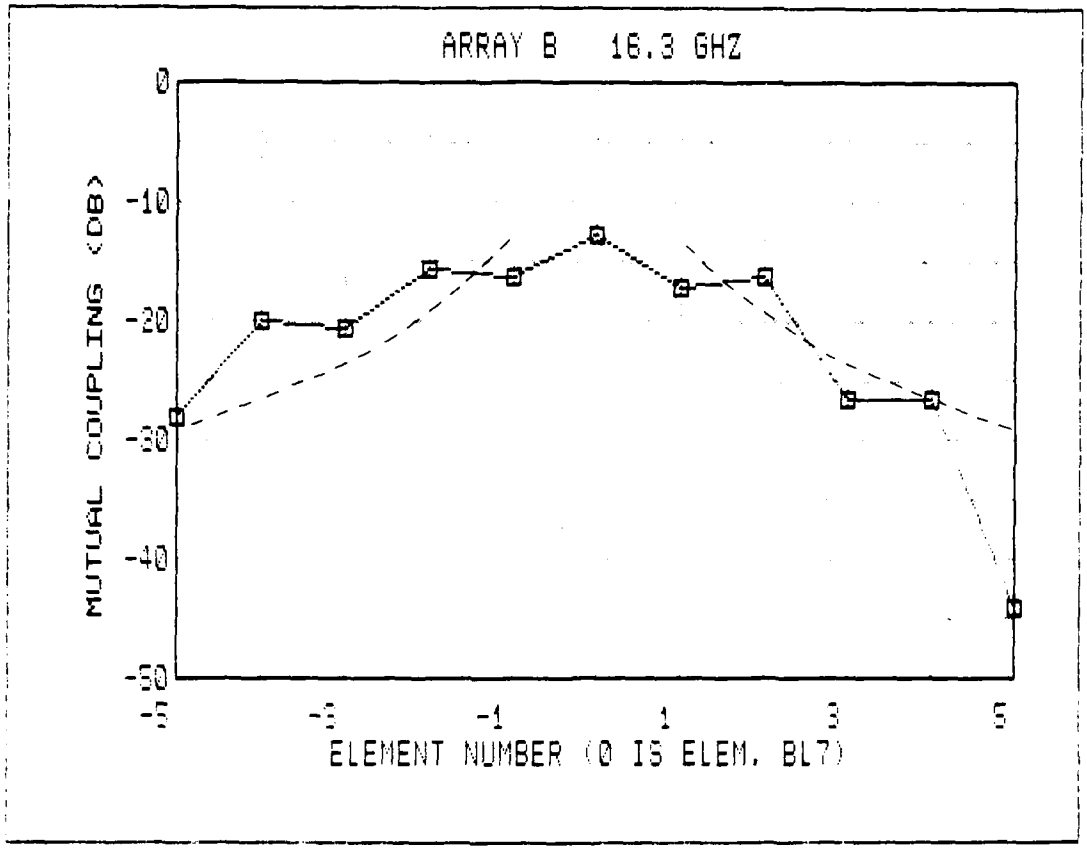

Figure 12b. Coupling Coefficient Magnitudes, $|S_{5,n}|$, From Array B (dashed line is typical microstrip array)

There are several possible sources of error that may explain the lack of clear results. First, we recently learned that Epsilam-10 is not an isotropic material—its dielectric constant is a function of direction, equalling 10 in the z direction (perpendicular to the substrate) but being closer to 13 in the x and y directions. Second, the material may not be uniform, but may have a variation in the dielectric constant over the same piece of material.

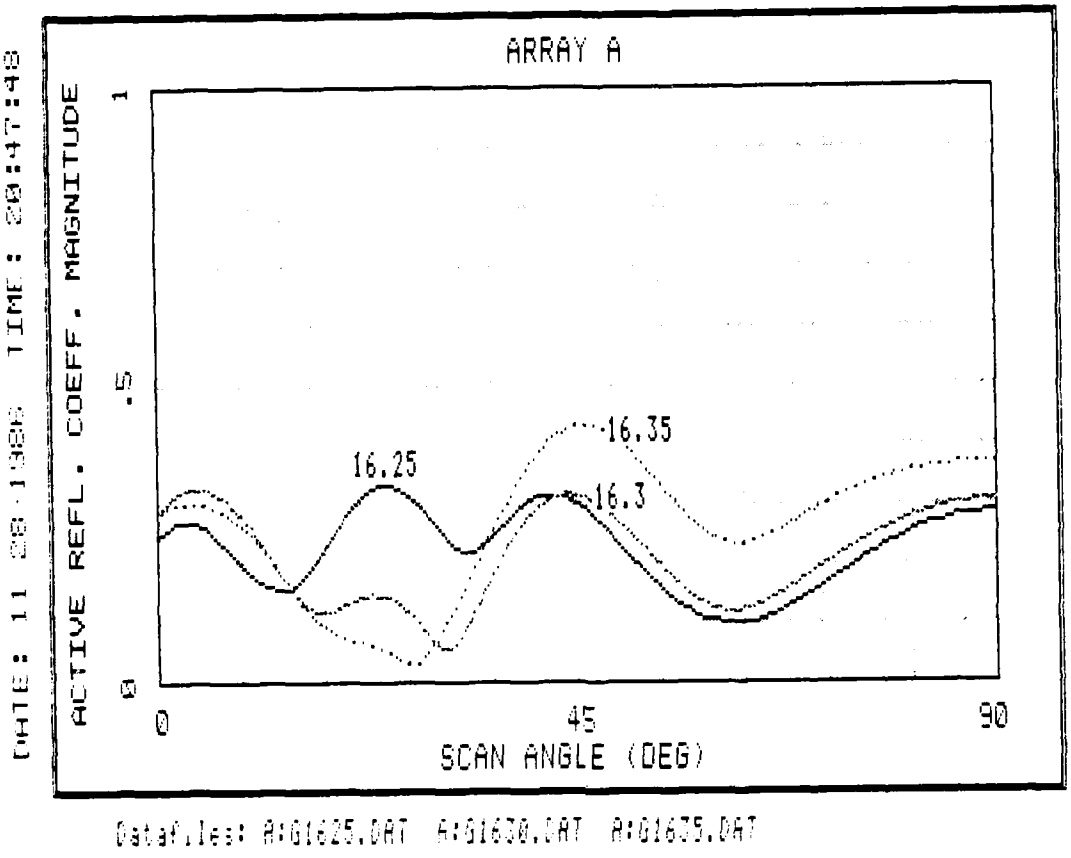

Figure 13a. Reflection Coefficient Magnitude vs Scan Angle at 16.25, 16.3 and 16.35 GHz: Array A

Figure 14 shows the measured resonant frequencies of a set of single rectangular patch antennas etched on the same piece of material as Arrays A and B. The solid and dashed lines in the figure are the resonant frequencies we would expect given dielectric constants of 10.0 and 13.0, respectively. Since the actual resonances do not follow either one exactly, we conclude that there may be some variation in the material's dielectric constant within the piece we used. That may explain why the two arrays gave such disparate results.

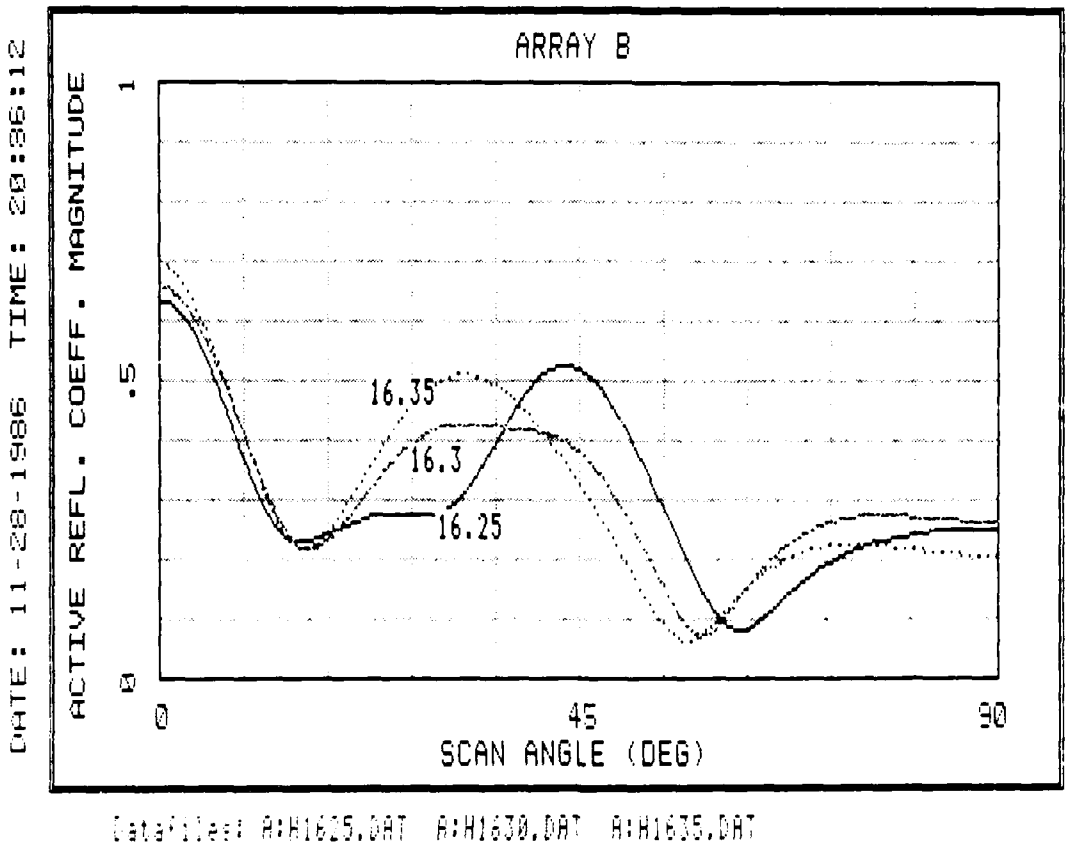

Figure 13b. Reflection Coefficient Magnitude vs Scan Angle at 16.25, 16.3, and 16.35 GHz: Array B

3.4 Modified (Probe-fed) Array

We surmised that some of the difficulties with the two arrays was due to the microstrip transmission line feeds with their accompanying coax-to-microstrip transitions and mitered bends. The poor impedance match to the 50-Ω transmission line presented by the patch with its inset region filled in could cause a series reflection with the miter and the transition. These reflections could add constructively and destructively in an unpredictable manner. In order to suppress these effects we modified Array A by trimming off the microstrip feed lines and feeding the elements from the back with coaxial probes as illustrated in Figure 15. Figure 16 is a photograph of the modified array. The probe center conductors are soldered to the patches at one edge. The elements' resonant frequencies were consistently near 14.7 GHz.

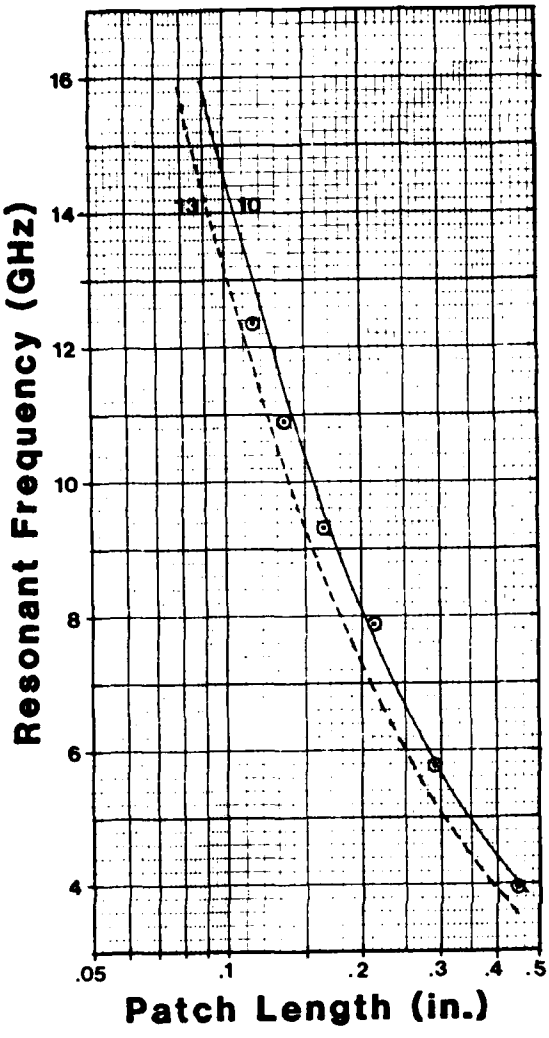

Figure 14. Measured Resonant Frequencies of Single Patch Elements on Epsilam 10

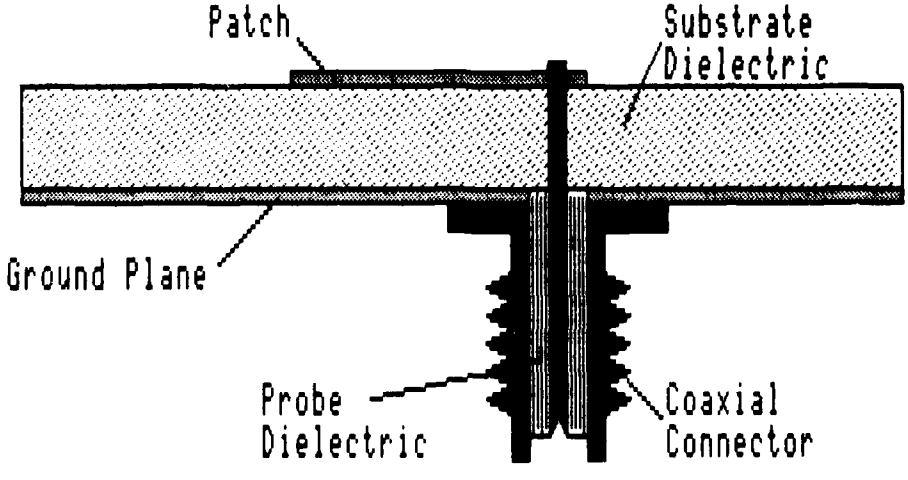

Figure 15. Method of Feeding a Microstrip Antenna With a Coaxial Probe

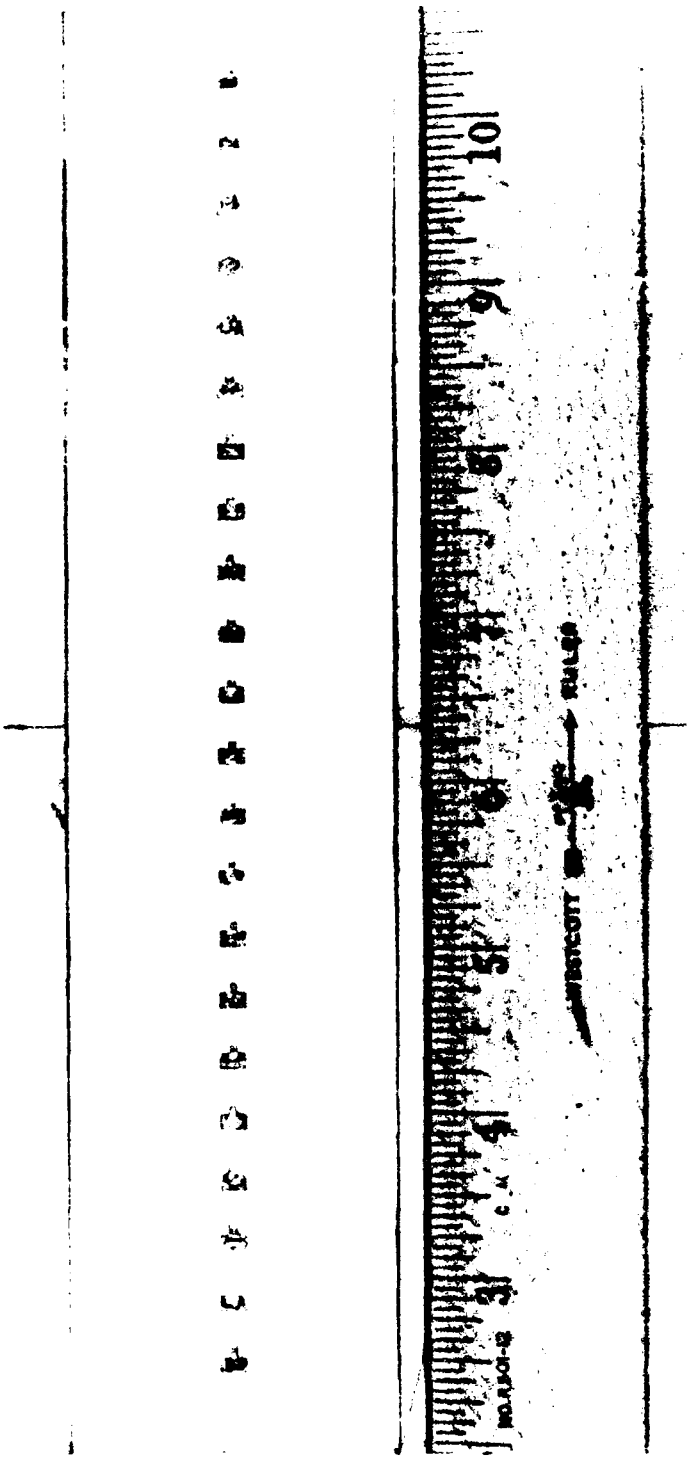

Figure 16. Modified Array With Probe-fed Elements

Figure 17 is the calculated $\Gamma(0)$ vs frequency. The array is clearly well matched over about a 5 percent bandwidth centered at 14.65 GHz. Figure . shows the scan reflection coefficients for 14.65, 14.7, and 14.75 GHz. The array goes blind near a 55° scan angle. In contrast to the original arrays there is very little attenuation in the coaxial lines feeding this modified array and we can therefore expect to measure reflection coefficients as high as 1.0. We have eliminated the broadside scan blindness observed in the original arrays since the only coupling path is now from one element to the next, and there is no chance of excess coupling between feed lines. Figure 19 shows the blind angle calculated from Eqs. (9) and (12) for dielectric constants of 10 and 13. Assuming the dielectric constant in the laterial direction is 13, the blindness observed in Figure 18 is in fact due to the surface wave.

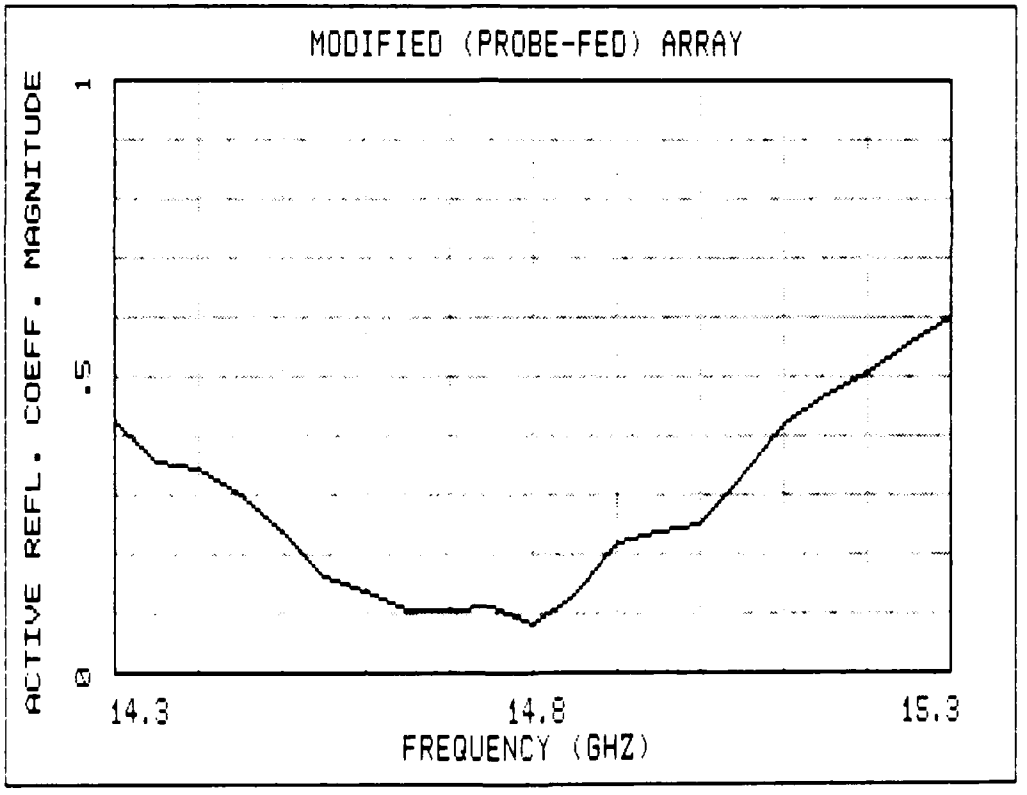

Figure 17. Broadside Scan Active Reflection Coefficient Magnitude $|\Gamma(0)|$ vs Frequency for Modified Array

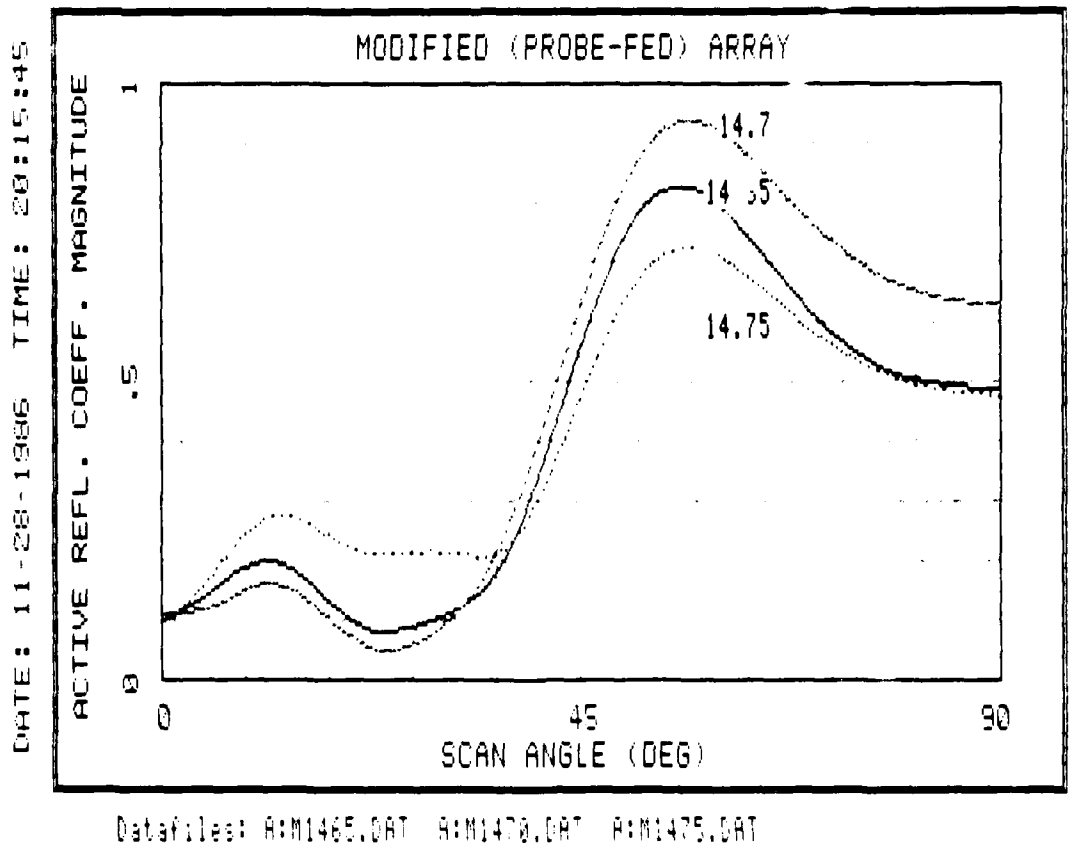

Figure 18. Reflection Coefficient Magnitude vs Scan Angle at 14.65, 14.7, and 14.75 GHz for the Modified Array

Figure 19 also shows the angles at which the TM_o leaky wave (see Appendix A) would produce a partial blindness. These are the angles for which the real part of the leaky wave propagation constant, β_z equals that of the Floquet mode. Unlike the surface wave, the leaky wave radiates, or "leaks," energy into free space as it propagates along the substrate, so it cannot cause a complete blindness. Unfortunately, the scan angles at which the leaky wave might produce a peak in Γ_a only exist for a narrow frequency range, which was outside the resonant bandwidth of both the original and modified arrays. In the frequency range measured with the original arrays, the blind angles for the two wave types are too close together to distinguish, especially given that the leaky wave can only produce a partial blindness. Nor can we estimate the effect the microstrip feed lines had in supporting or suppressing either wave type, or in altering their propagation constants.

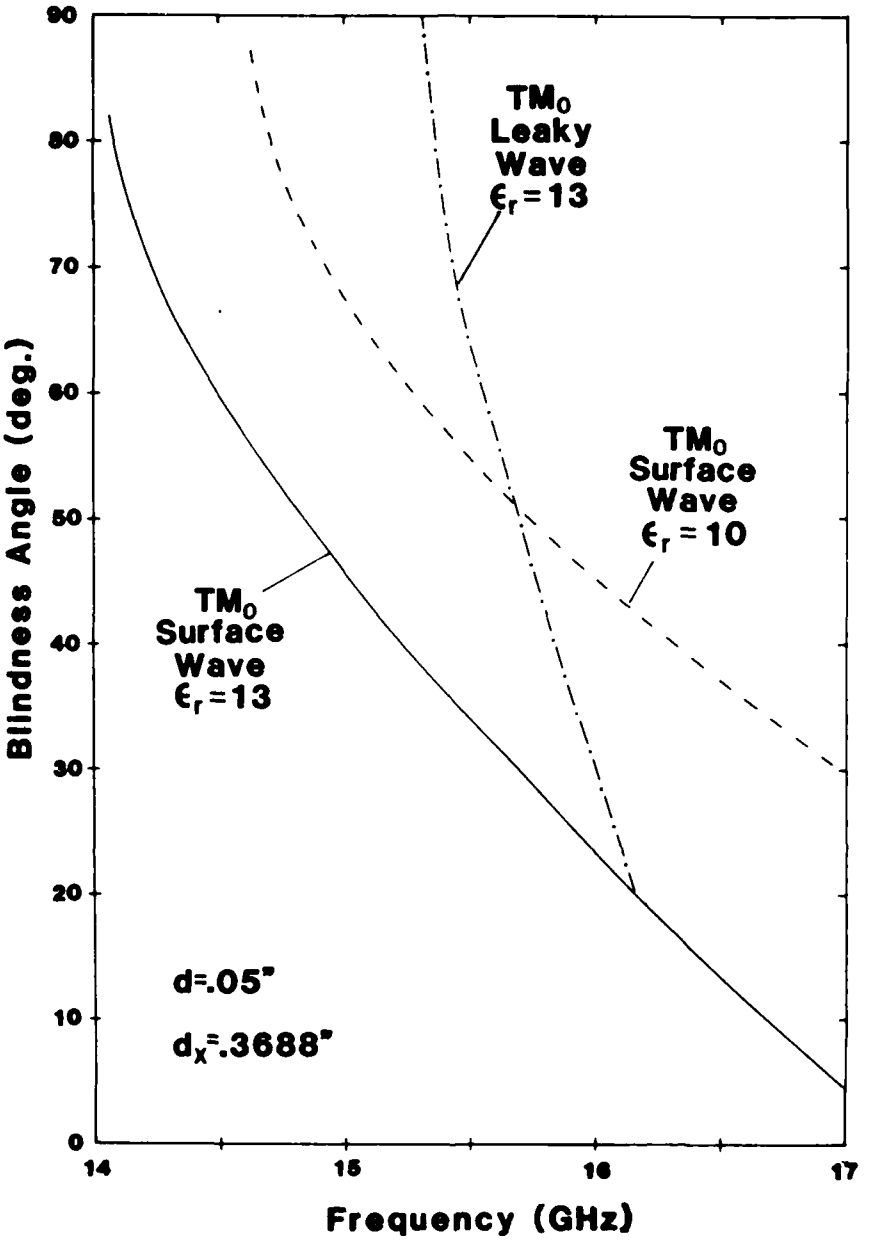

Figure 19. Scan Blindness for ϵ_r = 10.0 and ϵ_r = 13.0, Element Spacing = 0.3688 in., Substrate Thickness = 0.050 in.

Finally, Figure 20 is the pattern of one of the center elements of the modified array. Although the pattern does appear to roll off near the predicted blindness angle, there are too many other irregularities to be certain. We had to cement small pieces of microwave absorber to the ends of the array to smooth the pattern out to this extent, because the surface wave tends to radiate from the edge of the substrate. It is also possible that there is some additional radiation from the coaxial feeds, since they are not actually underneath the patches, but off to one side. These measurements made it clear to us that in order to get unequivocal results we need to construct a new array on a larger piece of more rigid material (Stycast Hi-K® for example), preferably one that is more uniform; and with an element designed to be fed with a coaxial probe. The coaxial feed is preferable to a microstrip feed line for this kind of experiment because the feed lines create and additional loading of the surface that may change β_{SW}, and hence also the blindness angle, as well as the effect discussed earlier of direct coupling between adjacent feed lines.

4. CONCLUSIONS AND RECOMMENDATIONS

One of the original objectives of this project was met successfully in that the scan blindness theory was verified. Our measurements on the modified (probe-fed) array showed a very clear scan blindness at the angle predicted by the theory. The earlier array did not show the blindness conclusively because of stray coupling between the microstrip feed lines. In general, the substrate material is very difficult to work with because it is flexible, and curvature effects will tend to corrupt any measurement of array mutual coupling. We did not attempt the second experimental objective (to suppress the blindness by forming obstructions in the substrate) although it is still a worthwhile experiment, but should begin with a re-designed array to eliminate the uncertainty involved in our element modifications (filling in the inset feed region). On the other hand, the theory shows that surface wave blindness should not be a problem given the very thin substrates we anticipate using for monolithic millimeter wave antennas for 44 and 60 GHz.

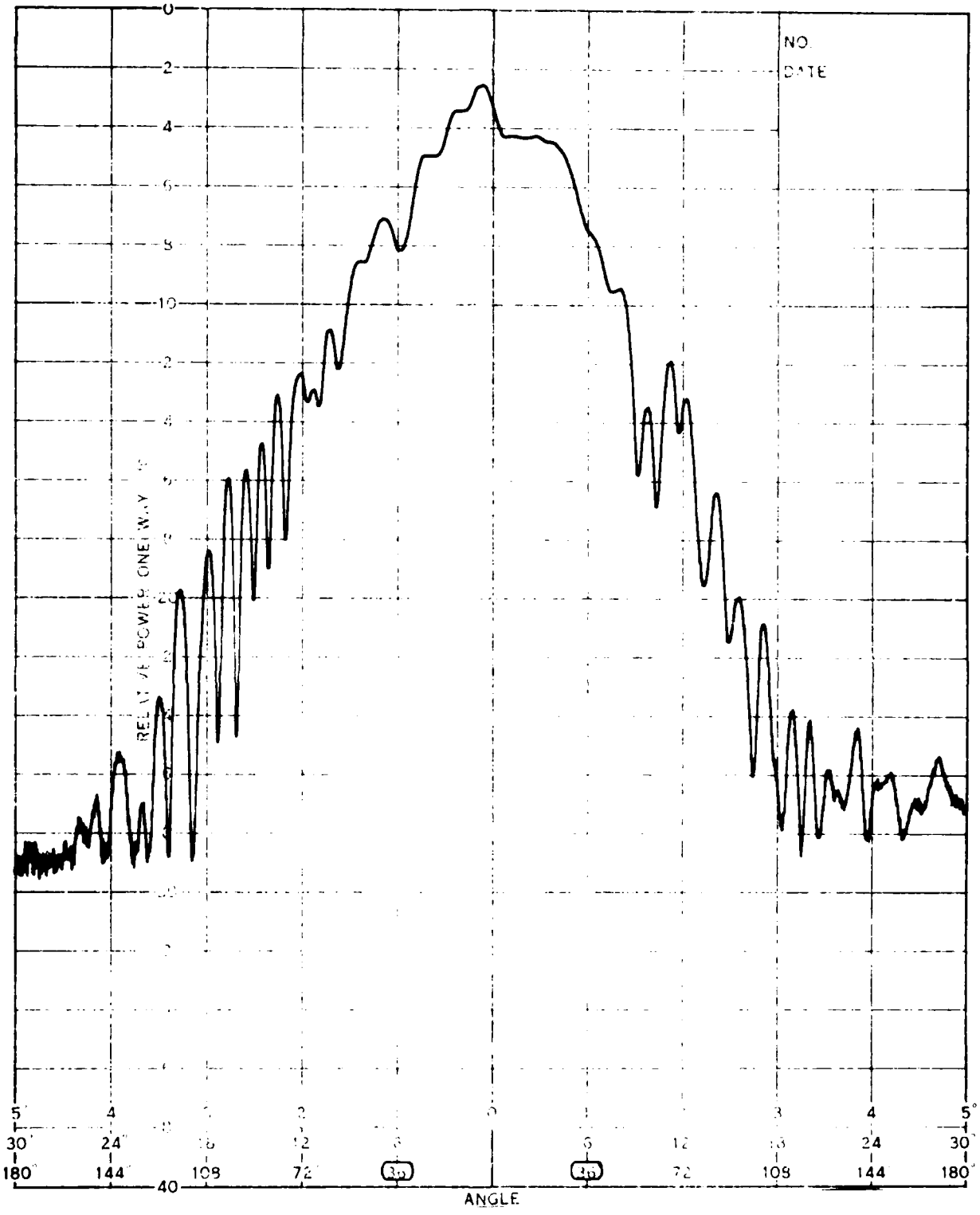

Figure 20. Imbedded Element Pattern, Central Element of Modified Array, 14.65 GHz, E Plane

References

1. Schindler, J.K. (1985) Performance bounds on monolithic phased array antennas, Phased Arrays 1985 Symposium Proceedings, RADC-TR-85-171, AD A169316, pp. 49-76.

2. Edward, B.J. (1984) Integration of monolithic microwave integrated circuits into phased array antenna systems, Proceedings of the 1983 Antenna Applications Symposium, *RADC-TR-84-52, AD A142003, pp. 39-64* Vol. I.

3. Bahl, I.J., and Bhartia, P. (1980) Microstrip Antennas, Artech House.

4. Pozar, D.M., and Schaubert, D.H. (1984) Scan blindness in infinite arrays of printed dipoles, IEEE Trans. Antennas Propag., AP-32;602-610.

5. Lee, S.W., Wong, N.S., and Tang, R. (1972) Analysis of infinite planar array of rectangular waveguides by generalized scattering matrix approach, Phased Array Antennas, Ed. Oliner and Knittel, Artech House, pp. 91-106.

6. Oliner, A.A. (1972) Surface-wave effects and blindness in phased array antennas, Phased Array Antennas, Artech House, pp. 107-112.

7. Amitay, N., Galindo, V., and Wu, C.P. (1972) Theory and Analysis of Phased Array Antennas, Wiley.

8. Mailloux, R.J. (1982) Phased array theory and technology, Proc. IEEE, 70:246-292.

9. Pozar, D.M., and Schaubert, D.H. (1984) Analysis of an infinite array of rectangular microstrip patches with idealized probe feeds, IEEE Trans. Antennas Propag., AP-32:1101.

10. Harrington, R.F. (1961) Time-Harmonic Electromagnetic Fields, McGraw-Hill, pp. 169-170.

11. Carver, K.R., and Mink, J.W. (1981) Microstrip antenna technology, IEEE Trans. Antennas Propag., AP-29:2-24.

12. Mullinix, D.A., and McGrath, D.T., Capt., (1986) Rectangular Microstrip Patch Antenna Arrays, RADC-TR-86-151.

References

A1. Zucker, F.J. (1971) Surface- and Leaky-wave antennas, Chapter 16, Antenna Engineering Handbook, 1st Ed., Ed. by H. Jasik, McGraw-Hill.

A2. Hessel, A. (1969) General characteristics of travelling wave antennas, Chapter 19, Antenna Theory Part 2, Ed. by R.E. Collin and F.J. Zucker, pp. 151-258, McGraw-Hill.

Appendix A

Solutions for Surface and Leaky Wave Propagation Constants

A1. TERMINOLOGY

The terms "surface wave" and "leaky wave" refer to mechanisms by which waves are guided along a boundary between any material and free space. With x and z the directions, normal to and parallel to the boundary, respectively, the surface wave has a purely real propagation constant in the z direction, and purely imaginary (decay) in the x direction. A leaky wave has complex propagation constants in both directions, with the added condition that the imaginary part in the x direction is negative.[A1]

A phased array antenna should, in general, be able to support both types of waves whether or not there is a dielectric layer over it. This is due merely because the array elements form a material boundary with free space. Some confusion arises from the fact that when an array is scanned to a blind spot, there is no energy radiated—it all propagates along the array surface, and the fields over the array surface are similar to those of a surface wave.[6] If that blindness is only partial, there will be some propagation along the surface and some radiation into free space, and the fields over the array surface will be similar to those of a leaky wave. The confusion is due to a failure to distinguish between these wave

A1. Zucker, R.J. (1971) Surface- and leaky-wave antennas, Chapter 16, Antenna Engineering Handbook, 1st Ed., Ed. by H. Jasik, McGraw-Hill.

modes set up by a blindness condition, and a blindness condition allowed by the natural tendencies of the particular material boundary to support surface or leaky wave modes. In this report, we were mainly concerned with the latter phenomenon: The array surface can support surface waves, that are therefore a mechanism by which the array elements can couple, and since the coupling is through a slow wave, a scan blindness can result. The surface waves exist all the time, not just when the array is scanned to a blind spot because they are a consequence of the dielectric slab forming the microstrip array's substrate. Since a dielectric slab can also support leaky waves, we cannot rule out the possibility that they might provide yet another coupling mechanism that will cause at least a partial blindness.

We have occasionally referred to a "leaky wave blindness," but since the leaky wave decays in the direction parallel to the array surface, it cannot cause a complete blindness. However, we shall, for convenience, refer to the angle at which the leaky wave produces a peak in the active reflection coefficient as a blindness angle.

This appendix reviews the classical model of the grounded dielectric slab used to solve for the propagation constants of surface wave and leaky wave modes. It shows that for any dielectric coated conductor, at least one leaky wave solution exists at any given frequency up to a critical frequency, where the slab's electrical thickness is $0.25\,\lambda$. Above that frequency the TM_o leaky wave ceases to exist. We have also found that the real part of the leaky wave's propagation constant is always smaller than that of the surface wave, and consequently, the scan blindness due to the leaky wave always appears at an angle greater than that of the surface wave.

A2. GROUNDED DIELECTRIC SLAB MODEL

The best-known method of solving for propagation constants of surface waves and leaky waves is based on finding a surface impedance. As illustrated in Figure A1 the grounded dielectric slab (GDS) is modelled as a shorted section of transmission line[A1] with characteristic impedance Z_o. The impedance of a short-circuited line transformed a distance ℓ back along the line is

$$Z_s = Z_o [j \tan (\beta \ell)] \tag{A1}$$

that is assumed to be the surface impedance of the dielectric seen looking down from the surface when $\beta \ell = dk_{xd}$, where k_{xd} denotes the propagation constant in the dielectric in the direction normal to the surface. The characteristic

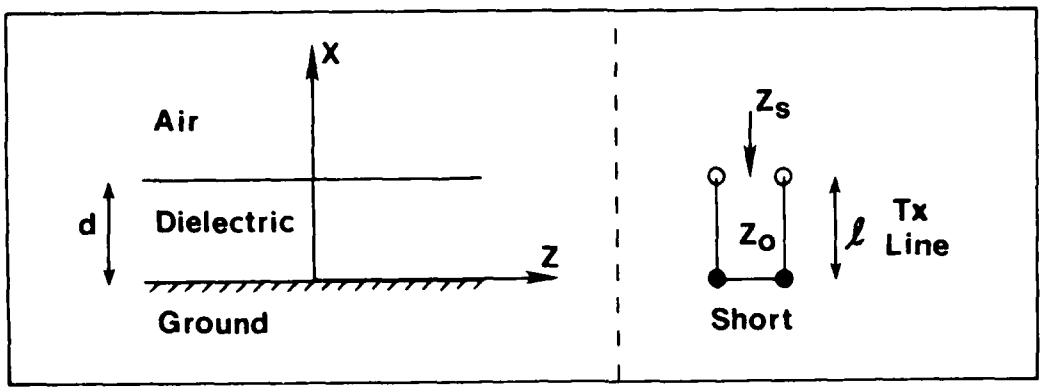

Figure A1. Transmission Line Analogy for the Grounded Dielectric Slab

impedance Z_o is the wave impedance, which depends on whether the mode is TM (magnetic field lines parallel to the ground plane) or TE (electric field parallel to ground):

$$Z_o = \begin{cases} k_{xd}/\omega e_1 & \text{(TM)} \\ \omega \mu_1 / k_{xd} & \text{(TE)} \end{cases} . \qquad \text{(A2)}$$

Since "wave impedances" normal to a material boundary must be continuous [Ref. 10: p. 55] we have $Z_s = -Z_x$, where Z_x represents the free space wave impedance. This is the well-known "transverse resonance relation".[A2] Note that it does not recognize possible loading of the surface by conducting objects, such as microstrip feed lines or antenna elements. So, for a real microstrip array, we can only consider this method approximate. It will be most accurate in cases where the dielectric constant is high and the patch antennas occupy only a small part of the slab's surface area.

The free space wave impedances are

$$Z_x = \begin{cases} k_x/\omega e_o & \text{(TM)} \\ \omega \mu_o / k_x & \text{(TE)} \end{cases} . \qquad \text{(A3)}$$

A2. Hessel, A. (1969) Characteristics of travelling wave antennas, Chapter, 19, Antenna Theory Part 2, Ed. R.E. Collin and F.J. Zucker, pp. 151-258, McGraw-Hill.

Substituting the wave impedances into Eq. (A1):

$$\frac{k_x}{\omega e_o} = j \frac{k_{xd}}{\omega e_1} \tan(dk_{xd}) . \qquad (A4)$$

In the dielectric, $k_{xd}^2 + k_z^2 = \epsilon k_o^2$, so $k_{xd} = \sqrt{\epsilon_r k_o^2 - k_z^2}$. For surface waves, there is no propagation in x and no attenuation in z and therefore $k_x = -j\alpha_x$ and $k_z = \beta_z$. The separability condition is $k_o^2 = k_x^2 + k_z^2$, from which we find $\alpha_x = \sqrt{\beta_z^2 - k_o^2}$, and substituting into Eq. (A4):

$$T_m = \epsilon_r \sqrt{\frac{\beta_z^2 - k_o^2}{\epsilon_r k_o^2 - \beta_z^2}} - \tan(d\sqrt{\epsilon_r k_o^2 - \beta_z^2}) . \qquad (A5)$$

Values of β_z that solve $T_m = 0$ are the surface wave propagation constants.

A3. LEAKY WAVE SOLUTIONS

For leaky waves, both k_x and k_z are complex and α_x is negative: $k_z = \beta_z - j\alpha_z$, $k_x = \beta_x - j\alpha_x$. A more convenient form of Eq. (A5) is:

$$T_m = \epsilon_r \sqrt{\frac{k_z^2/k_o^2 - 1}{\epsilon_r - k_z^2/k_o^2}} - \tan\left[k_o d \sqrt{\epsilon_r - k_z^2/k_o^2}\right] \qquad (A6)$$

Leaky wave solutions are those combinations of α_z and β_z for which both real and imaginary parts of T_m are zero. Figure A2 shows $Re[T_m]$ and $Im[T_m]$ vs β_z for a few values of α_z. Figure A3 shows the solutions for α_z, β_z and β_{SW} for substrate with thickness d = 0.05 in. and dielectric constant $\epsilon_r = 13$ (some example values are given in Table A1). This figure brings out four very important facts:

(1) the transverse propagation constant of the leaky wave is asymptotic to that of the surface wave, that is, the leaky wave is always faster than the surface wave;

(2) above that frequency where $\beta_z = \beta_{SW}$ the leaky wave does not exist and that critical frequency is given by $0.25\,\lambda_c = d\sqrt{\epsilon_r}$;

(3) up to that frequency a leaky wave can always exist; however,

(4) the imaginary part of α_z is so large for lower frequencies that it will attenuate very quickly instead of propagating along the surface, and will therefore be a weak mechanism for mutual coupling.

When an array is placed on the dielectric slab, the phase of the mutual coupling will be determined by β_z and β_{SW}. The leaky wave can cause a strong array reflection when $\beta_z = \beta_{fm}$, that is, the propagation constant of the Floquet mode. That "blind" angle is

$$\theta_{LWB} = \sin^{-1} (\lambda / d_x - \beta_z / k_o) . \tag{A7}$$

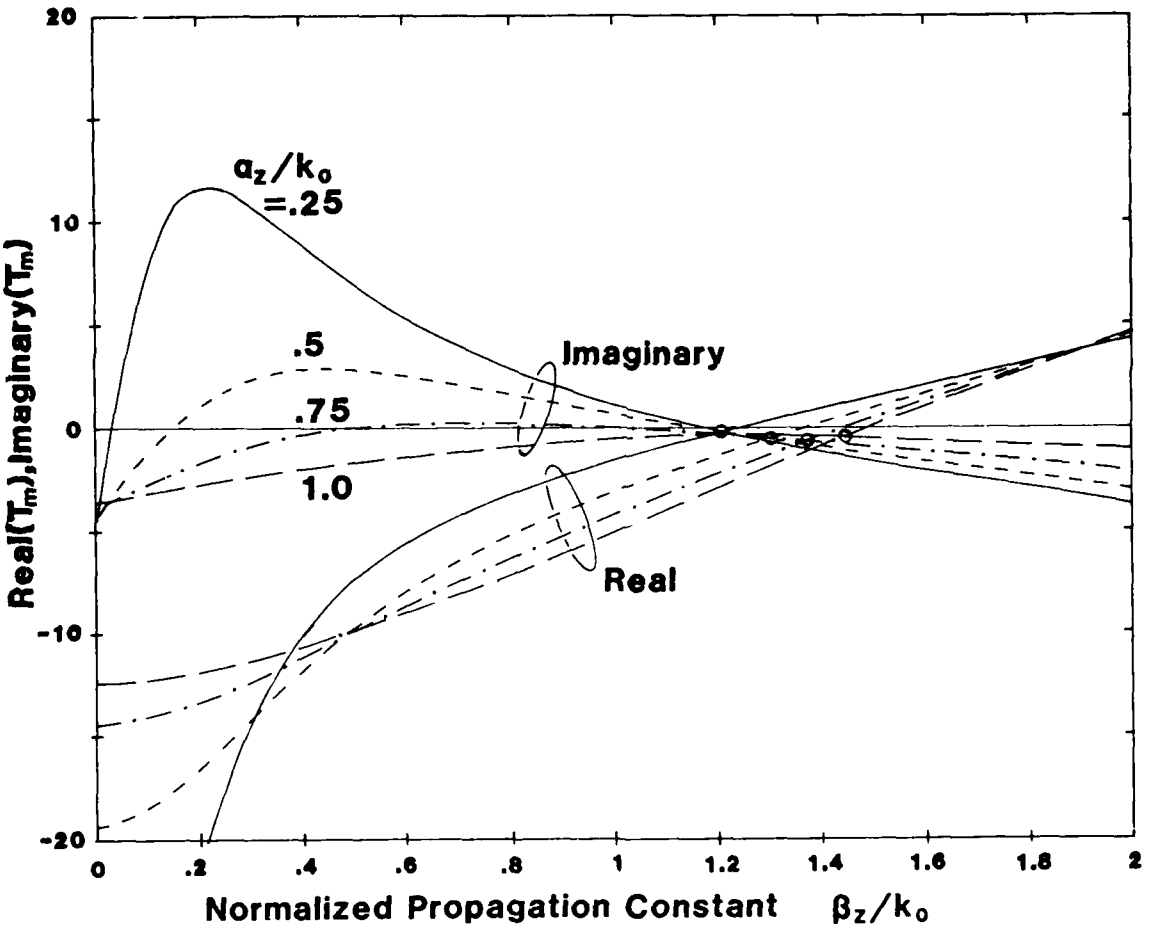

Figure A2. Real and Imaginary Parts of T_m vs β_z for f = 15.5 GHz, ϵ_r = 13, and d = 0.05 in.

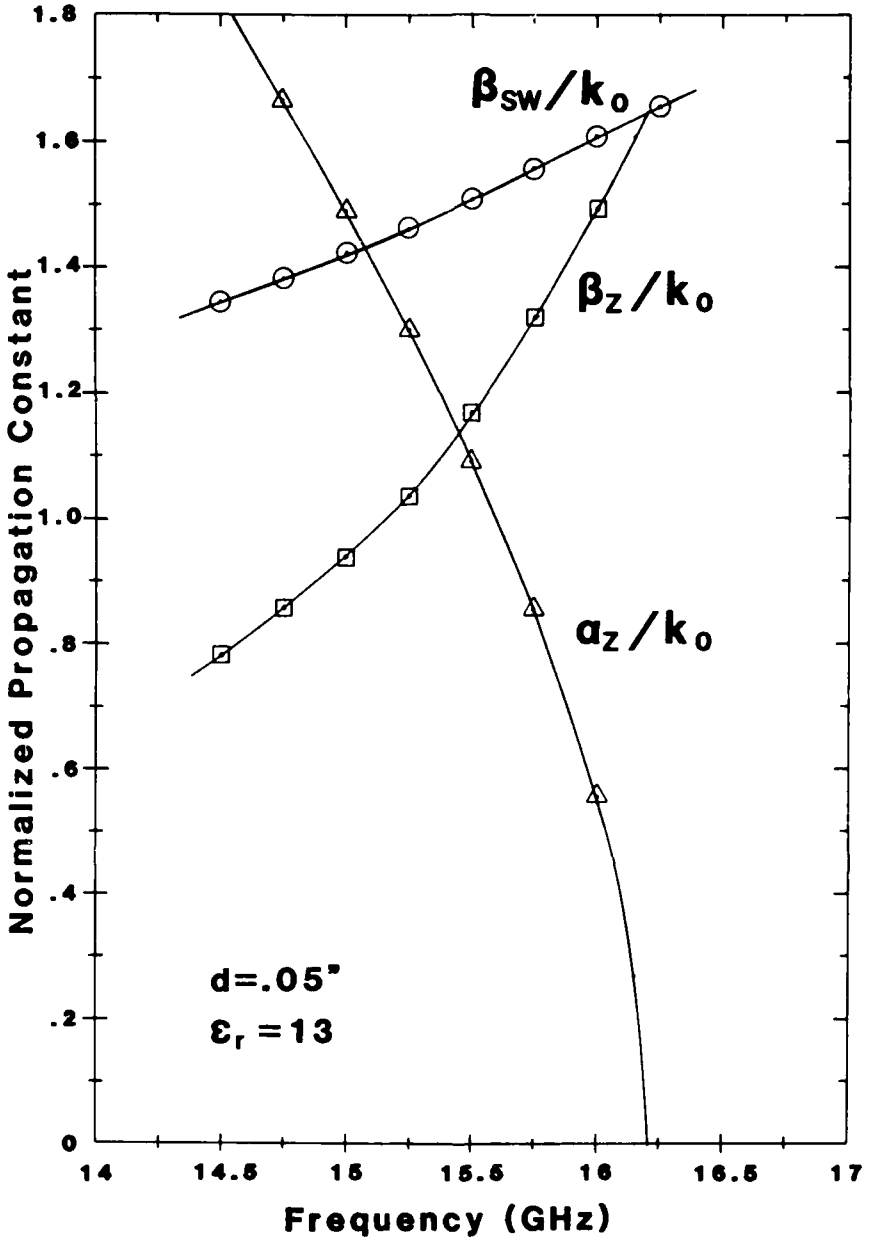

Figure A3. Solutions for α_z, β_z and β_{SW} for a Grounded Dielectric Slab With d = 0.05 in. and ϵ_r = 13

Table A1. Example Solutions for Leaky Wave Propagation Constants for a Grounded Dielectric Slab With d = 0.05 in. and ϵ_r = 13, TM_0 Mode

Frequency (GHz)	$\frac{\alpha_z}{k_o}$	$\frac{\beta_z}{k_o}$	$\frac{\beta_{SW}}{k_o}$
14.50	1.827	0.780	1.344
14.75	1.661	0.854	1.381
15.00	1.486	0.934	1.421
15.25	1.298	1.035	1.463
15.50	1.092	1.165	1.508
15.75	0.856	1.319	1.556
16.00	0.555	1.495	1.604
16.25	0.0	1.654	1.654

Figure 19 shows that a leaky wave blindness is only possible for a very narrow range of frequencies for our substrate (15.5 to 16.25 GHz). Unfortunately, this range was outside the resonant bandwidths of both the original arrays and the modified array, so our experimental data cannot show either the existence or lack of a leaky wave blindness.

However, it is very important to note that the leaky wave blindness angle is always greater than the surface wave blindness angle. We have noted previously that the surface wave only causes blindness in electrically thick substrates, and conclude that the same is true for the leaky wave. Furthermore, the leaky wave cannot cause a complete blindness (Γ = 1) since it does radiate instead of remaining attached to the surface. On the other hand, a complete microstrip phased array will have appreciable surface loading due to phase shifters, power splitters and transmission lines. The propagation constants of both wave types may be considerably altered by that loading, and the scan blindness may occur at lower frequencies than predicted by the analysis for the grounded dielectric slab.

END

DATE

FILMED

MARCH

1988

DTIC